Modulation of precipitation by a mesoscale gravity wave in northern Italy: Detection and analysis

Quarterly Journal of the Royal Meteorological Society
A journal of the atmospheric sciences and physical oceanography
RMetS

Modulation of Precipitation by a Mesoscale Gravity Wave in Northern Italy: Detection and Analysis

Journal:	*QJRMS*
Manuscript ID	QJ-19-0043.R1
Wiley - Manuscript type:	Research Article
Date Submitted by the Author:	26-Jul-2019
Complete List of Authors:	RICHIARDONE, Renzo; Università degli Studi di Torino, Dipartimento di Fisica Manfrin, Massimiliano; Università degli Studi di Torino, Dipartimento di Fisica Ferrarese, Silvia; Università degli Studi di Torino, Dipartimento di Fisica Campistron, Bernard; Observatoire Midi-Pyrenees, Laboratoire d'Aérologie, UMR5560 Klaus, Vladislav; Météo France Toulouse, CNRM GMEI/STM
Keywords:	modulation of precipitation, mesoscale gravity waves, shear instability, Kelvin-Helmholtz instability, wave ducting, tropospheric jet, stability analysis, microbarometer
Country Keywords:	Italy

ORIGINAL ARTICLE
Journal Section

Modulation of Precipitation by a Mesoscale Gravity Wave in Northern Italy: Detection and Analysis

Renzo Richiardone[1] | **Massimiliano Manfrin**[1] | **Silvia Ferrarese**[1] | **Bernard Campistron**[2] | **Vladislav Klaus**[3]

[1]Università di Torino, Dipartimento di Fisica, Torino, Italy

[2]Laboratoire d'Aérologie,UMR5560, Observatoire Midi-Pyrénées, Toulouse, France

[3]Météo-France - CNRM GMEI/STM, Toulouse, France

Correspondence
Renzo Richiardone, Dipartimento di Fisica, Università di Torino, via Giuria 1, 10125 Torino, Italy
Email: richiardone@ph.unito.it

Funding information
CNR, Grant Number 97.04798.ST74

A 6-h event of increased and gravity-wave modulated stratiform rain with a period of approximately 1 h is described and two wave generation mechanisms (geostrophic adjustment and shear instability) are investigated. The predictions of a linear stability analysis of the flow (an unstable mode of about 100-km wavelenght originating from the shear instability of the tropospheric jet and propagating in a duct encompassing almost the entire troposphere) are shown to agree very well with the measurements from a microbarometer network and wind-profiler soundings.

KEYWORDS
modulation of precipitation, mesoscale gravity waves, shear instability , Kelvin-Helmholtz instability, wave ducting, tropospheric jet, stability analysis, microbarometer

1 | INTRODUCTION

The interest in the influence of Mesoscale Gravity Waves (MGWs, waves with wavelength $\geq$ 50 km and period $\geq$ 1 h) on precipitation has increased in recent decades along with the increased coverage of weather radars and surface-measurement networks. It is well known that when the atmosphere is conditionally unstable, atmospheric gravity waves can trigger thunderstorms and produce rain bands. Less well-documented is the effect of MGWs on precipitation under stable conditions. The present analysis is of such a case, which occurred on 21 Oct 1999 in northern Italy.

Uccellini and Koch (1987) reviewed of 13 cases to identify a common synoptic-scale environment within which MGWs are generated. Koch and Siedlarz (1999) identified coherent pressure-pulse events with periods of 1-6 h on 32%

of the days during the six weeks of the STORM-FEST (STORM Fronts Experiment System Test) in the central United States, a frequency that they compare to that of 21 % found by Grivet-Talocia et al. (1999) in central Illinois. During the same experiment, an episode of MGWs that exerted a strong influence on the precipitation distribution in a large area was analyzed by Trexler and Koch (2000) and Jewitt et al. (2003). A very well-documented event that has been thoroughly investigated (Koch and Golus (1988), Koch et al. (1988),Koch and Dorian (1988), Koch et al. (1993) and Kaplan et al. (1997)) occurred during the Cooperative Convective Precipitation Experiment (CCOPE). Other events of MGW influence on the precipitation were analyzed by Bosart and Seimon (1988), Ferretti et al. (1988), DeMaria et al. (1989), Ralph et al. (1993), Zülicke and Peters (2007) , Houser and Bluestein (2011), Ruppert Jr and Bosart (2014) and Wu et al. (2015). Some of them have also been studied by means of numerical simulations (Powers and Reed (1993), Kaplan et al. (1997), Zhang et al. (2001), Zülicke and Peters (2007), Zhang et al. (2013)). Studies of MGW influence on convective-precipitation episodes are more numerous than those on stratiform precipitation, probably because convective events can have important impacts on society and can also be detected more easily, both for their intensity and for the spatial signature caused by the triggering action of the wave.

Many of the above-cited events occurred in synoptic settings that Uccellini and Koch (1987) suggested as favorable for MGW development: a strong thermal inversion in the lower troposphere, usually on the cool side of a warm or stationary front and a jet streak (an isotach maximum embedded within a jet stream, Palmén and Newton (1969)) propagating toward a ridge axis in the upper troposphere. Regarding possible mechanisms for MGW generation, Uccellini and Koch (1987) suggest shear instability of the upper-level jet or geostrophic adjustment in the exit region of the jet streak. Both mechanisms, not mutually exclusive but sometimes cooperating (Koch et al. (1993)), have been proposed in the above-cited papers. A thorough review of gravity-wave generation from atmospheric jets can be found in Plougonven and Zhang (2014).

A question concerns how MGWs, whatever the process may be for its generation, can last for many hours propagating in a coherent fashion without appreciable changes over a distance of roughly a thousand kilometers. A primary ingredient for long-lasting MGWs is the existence of a wave duct in which the wave can propagate horizontally without great loss of energy and hence without the need for a continual supply of energy. Lindzen and Tung (1976), by means of a simple three-layer model, showed that an effective duct can exist when a stable layer adjacent to the ground is capped by a dynamically unstable sheared layer with Richardson number Ri < 0.25 and contains a critical level, i.e., a level where the unperturbed flow speed is equal to the phase speed of the wave. They also showed that, in some ranges of very small Ri, even a slight overreflection of all MGW wave modes can occur. In this case the wave would grow in amplitude by extracting energy from the mean flow in the absence of dissipative mechanisms. A critical level is frequently observed in MGW events. The existence of a critical level is an additional support for the shear-generation mechanism, since the critical level can not only act to duct the wave energy, but can also serve as a generation mechanism for the MGW, provided the local shear is sufficiently strong that Ri<0.25 (Stobie et al. (1983), Uccellini and Koch (1987)).

The purpose of this paper is to analyze in detail the event of MGW-modulated stratiform precipitation described in Richiardone and Manfrin (2003) and to investigate the wave-generation mechanism. The episode occurred under conditions of large near-ground atmospheric stability, i.e., very far from convective conditions. The event occurred in northern Italy on 21 October 1999 (Richiardone and Manfrin (2003)) during Intensive Observing Period 8 (IOP8) of the Mesoscale Alpine Programme (MAP; Bougeault et al. (2001), Volkert and Gutermann (2007)). One of the primary MAP objectives was the study of precipitation events in the vicinity of complex topography, and one of the target areas was located in the Po Valley, to the south of the Alps. The Atmospheric Physics group of Turin University participated in the MAP experiment by installing a microbarometer network and a high-precision pluviometer in the western part of the Po Valley in order to study the gravity-influence influence on precipitation (Richiardone et al. (2001)).

The present analysis of the event is based on microbarometer and pluviometer measurements at ground level and

upper-air measurements from radio soundings and wind profilers. The experimental setup is described in Section 2 and the episode (data and synoptic background) in Section 3. The hypotheses about the wave generation are discussed in Section 4 (Geostrophic Adjustment) and Section 5 (Shear Instability). Section 5 contains also the comparison between the observations and the theoretical predictions of a linear stability analysis. It is followed by the conclusions in Section 6.

2 | EXPERIMENTAL SETUP

In northern Italy the Po Valley extends eastward from the French border to the Adriatic sea, bounded on the north by the Alps and on the south by the Apennines. During the MAP experiment, the Turin University group deployed a microbarometer network in the western part of the Po Valley. This network was composed of a three-station subnetwork in Torino (TOR), another in Trino Vercellese (TRI) and one station in Agliè (AGL) (Fig. 1). In both three-station subnetworks, the microbarometer stations were situated a few kilometers apart to form an approximately equilateral triangle. Differential microbarometers, allowing the measurement of pressure fluctuations with periods from 5 s to 18 h, with corresponding resolutions from 0.2 Pa to 2.0 Pa, were used (Richiardone (1993)). These instruments correctly measure pressure fluctuations with a period ranging from 5 *s* to 20 min. The amplitudes and phases of longer period fluctuations must be reconstructed from the sensor output by means of the instrument transfer function.

In each of the three sites, absolute atmospheric pressure was also measured to within an accuracy of 20 Pa using commercial barometers (SETRA, mod. 270).

High-resolution measurements of rain rate were made at one of the TRI stations (Valbischiera, 45.24° N, 8.27° E, TRI_VAL, hereafter) using a high-precision pluviometer (0.01 mm accuracy , mod. PLUVIO by OTT Hydrometrie). In order to eliminate vibrations and temperature fluctuations, the instrument continuously measured the weight of the precipitation-collection container and processed and output the data every minute. The temporal delay (270 s) introduced by its internal data processing was measured in the laboratory to avoid any systematic error in rain-intensity timing.

At Lonate Pozzolo (LON, 45.57° N, 8.72° E) Météo-France installed two (VHF and UHF) wind profilers (Fig. 1). The main characteristics of the VHF wind profiler were the following: a 45 MHz transmitted frequency, with a 12-kW peak power, a 6400-Hz pulse-repetition frequency, and a 375-m radial resolution. The radar used five beams (one vertical and four oblique with an off-zenith angle of 15°) of a 5.6° aperture. Vertical profiles of the three component of the wind were provided every 15 minutes, from 2 km up to 16 km (depending of the atmospheric conditions), with a 375-m vertical sampling. The main characteristics of the five-beam UHF-band wind profiler were the following: a 1294-MHz transmitted frequency, a 4-kW peak power, a 20-kHz mean pulse-repetition frequency and a 75-m radial resolution. The vertical beam and the four oblique beams (17° tilted from zenith) had the same aperture of 8.5°. With a dwell time of 5 minutes, the measurements provided the three wind components, with a 75-m vertical sampling between 75 m up to 3 km in clear air, depending on atmospheric conditions. The UHF profiler, contrary to VHF,is very sensitive in the detection of precipitation even very weak such as drizzle. Interested readers in wind profiler signal characteristic and processing can found a detailed explanation in Saïd et al. (2016).

3 | THE EPISODE

The MGW event occurred on the morning of 21 Oct 1999 between 0500 UTC and 1100 UTC, during a period of widespread stratiform precipitation south of the Alps. A Meteosat image (Fig. 2) shows that at 0800 UTC an arching

cloud band originating over North Africa marked an organized large-scale flow, enhanced by Mediterranean moisture, northward toward the Alps (Bousquet and Smull (2003)). The cloud band was associated with a frontal system that occluded on the morning of 21 Oct 1999 (Fig. 6c of Richiardone and Manfrin (2003)) . In the upper troposphere the 300-hPa height maps from the ECMWF analysis (Fig 3) showed from the previous day a good similarity to the schematic Uccellini and Koch (1987) model (Fig. 4) until 0000 UTC of 21 October, when the area between the inflection and the ridge axes (the area of greatest potential for MGW occurrence) became very narrow. At 0600 UTC of 21 October, one hour after the event start, it seems that the area further narrowed and just overstepped the TRI microbarometric network.

From 0500 to 1100 UTC simultaneous increases of rain rate and pressure fluctuations occurred at TRI_VAL (Fig. 5). Spectral analysis (not shown here) of both signals during this 6-h event showed significant (at the 5 % level) peaks, with periods of 66 ± 3 min in pressure and 64 ± 3 min in rain rate, in agreement with their autocorrelation. The cross-correlation between the raw, temporal-delay corrected rain rate signal and the raw pressure fluctuations signal was largest and significant at the 1 % level at time lag of 21 min, with the rain rate following the pressure (Figure 6).

Afterwards, three running means of order 3, 13 and 5 were successively applied to the rain rate signal to avoid any intermittence. All the signals were then filtered by applying a 55-75 min band-pass filter (MATLAB R2018b Parks-McClellan optimal equiripple FIR), and the pressure fluctuations signals were corrected for the microbarometer's transfer function (Richiardone (1993)) at the center of the band-pass window. Finite Impulse Response (FIR) filters guarantee that the phase relationships of the frequency components of the input signals are not distorted. After the filtering and the pressure correction, the cross-correlation between the rain rate and the pressure during the event resulted largest at time lags of 13 min and 14 min, with the precipitation following the pressure (Figure 7).

The pressure signals at the TRI subnetwork stations were analyzed by means of the so-called beamsteering method (Einaudi et al. (1989)) to evaluate the wave speed and direction that maximizes the average cross-correlation between the pressure measurements (if a couple of sensors measure the same periodic function of time, the cross-correlation coefficient between their signals reaches a value of 1 for an appropriate value of lag which depends on their relative position and on the speed and direction of propagation).

This analysis showed that at TRI, during the six hours of the event, a pressure wave traveled northward (direction of propagation of $0^\circ \pm 15^\circ$) with a speed of 25 ± 3 m s^{-1}. These values imply an estimated wavelength of 99 ± 16 km. In Fig. 7 the filtered pressure signals at AGL and TRI_FIS indicate a strong decrease in amplitude going westward from TRI. Further east, in contrast, the signature of a MGW with a wavelength of approximately 100 km was found in the turbulence measurements taken between 0600 and 0800 UTC by a research aircraft during a flight over the Alps between Italy and western Austria at the longitude of about 11° E (Jiang and Doyle (2004)).

During the event under discussion, the VHF wind profiler in Lonate Pozzolo measured an alignement of the wind velocity at the wave direction and an increase of the wind speed between 8 km and 11 km just when the pressure fluctuations at TRI reached their maximum amplitude (Fig. 8). Jet streaks being associated with enhanced vertical wind shear (Uccellini and Koch (1987)), this coincidence suggests the hypothesis that the wave could have been generated by a shear instability of the tropospheric jet stream, one of the possible mechanisms suggested by Uccellini and Koch (1987) for MGW generation. A comparison between the Fig 4 and the 300-hPa height at 0600 UTC (Fig 3) shows that the event occurred when the inflection axis almost coincided with the ridge axis and the jet streak pointed northward.

Another feature of the event that agrees with the Uccellini and Koch (1987) model and is favorable to the onset of a ducted wave is the strong thermal inversion in the Po Valley (Fig. 9) due to a persistent layer of a very stable, cool air mass near the ground, an important feature of MAP IOP8 (Rotunno and Houze (2007)).

4 | GEOSTROPHIC ADJUSTMENT

In the synoptic setting that Uccellini and Koch (1987) suggested as favorable for MGW development (Fig. 4), the upper-level jet streak propagates towards a ridge in the 300 hPa height field. By observing that 1) the upper-level flow regime which characterizes MGW wave events is similar to that has been deemed unbalanced and 2) that theoretical and model studies have indicated that gravity-inertia waves are a means to restore the atmosphere back toward a balanced state, Uccellini and Koch (1987) suggested that MGWs might be generated by a geostrophic adjustment process and maintained by ducting through a mechanism similar to that proposed by Lindzen and Tung (1976). Keeping the term "adjustment", some authors prefer to generalize the process using the terms of balance adjustment (Zhang (2004)), spontaneous adjustment emission (Ford et al. (2000), Wang and Zhang (2010)) or simply spontaneous emission (Plougonven and Zhang (2014)). The geostrophic adjustment paradigm has been often verified in the numerical investigations of the observed cases, as well as the numerical simulations of the idealized baroclinic waves (e.g. O'Sullivan and Dunkerton (1995), Zhang (2004), Plougonven and Snyder (2007), Wei and Zhang (2014)). The hypothesis of wave generation by geostrophic adjustment for the present case is tested in the following.

Various diagnostics have been proposed to evaluate if the flow is unbalanced over the apparent gravity-wave source region (Koch and Dorian (1988), Zhang et al. (2001)). The first (and often used, being the simplest) is the Lagrangian Rossby number Ro, defined as the ratio of parcel to Coriolis accelerations. Use of the frictionless equation of motion gives

$$Ro = \frac{d\boldsymbol{V}}{dt}\frac{1}{f\,|\boldsymbol{V}|} = \frac{|f\boldsymbol{V}_{ag}\times\boldsymbol{k}|}{f\,|\boldsymbol{V}|} = \frac{|\boldsymbol{V}_{ag}|}{|\boldsymbol{V}|} \approx \frac{\left|\boldsymbol{V}_{ag}^{\perp}\right|}{|\boldsymbol{V}|} \tag{1}$$

where f is the Coriolis force, $\boldsymbol{V}_{ag}^{\perp}$ is the component of the ageostrophic wind $\boldsymbol{V}_{ag} = \boldsymbol{V} - \boldsymbol{V}_g$ perpendicular to the wind vector $\boldsymbol{V}$, $\boldsymbol{V}_g$ is the geostrophic wind and $\boldsymbol{k}$ is the unit vertical vector (Zhang et al. (2001)). The latter approximation in this equation follows from Koch and Dorian (1988) who argued that only the ageostrophic wind normal to the flow is relevant to an assessment of flow imbalance, provided that the along-stream ageostrophic wind is governed by gradient wind balance (Zhang et al. (2001)). In order to diagnose if the flow is unbalanced, Koch and Dorian (1988) suggest to use the criterion

$$Ro \approx \frac{\left|\boldsymbol{V}_{ag}^{\perp}\right|}{|\boldsymbol{V}|} > 0.5 \tag{2}$$

in a region where $|\boldsymbol{V}| > 10$ m s^{-1} and the ageostrophic wind is directed toward the cyclonic side whose direction is within 45° of being normal to the observed wind. Only cross-stream ageostrophic flow directed toward the cyclonic side of the jet should be used to assess unbalanced flow in the exit region of the jet with formula (2), because it alone indicates that air parcels are accelerating when they should be decelerating to convert their excess kinetic energy to potential energy. This is the criterion that has been suggested to forecast a possible MGWs occurrence in operational forecasting (Koch and O'Handley (1997))

In order to investigate if the geostrophic adjustment could be responsible for the existence of the wave signals observed on 21 October 1999, the field of the Lagrangian Rossby number approximated in (2) has been analyzed to highlight the regions of unbalanced flow on 20 and 21 October. The meteorological fields have been derived using

the Weather Research and Forecast model (WRF, Skamarock et al., 2005), version 3.7, with horizontal grid-spacing of 9 km in the second of three nested domains and 40 vertical levels between the surface and the 50 hPa upper boundary. Input and boundary conditions were provided by ECMWF reanalysis of the MAP period (Keil and Cardinali (2004)). The 300 hPa geopotential height and wind velocity fields have been smoothed by twice applying a 2D running mean of order 29, and the geostrophic wind has been evaluated calculating the derivatives over 6 grid points, i.e. about 25 km along the longitude and 20 km along the latitude.

In order to evaluate the flow imbalance, two kinds of areas have been displayed in Figures 10 and 11 together with the geopotential height and the velocity fields:

1. Stippled areas, where the ageostrophic winds are deemed significantly unbalanced ($\boldsymbol{V}_{ag}^{\perp}$ directed toward the cyclonic side whose direction is within 45° of being normal to the observed wind $\boldsymbol{V}$, provided that $|\boldsymbol{V}| > 10$ m s^{-1} as in Koch and Dorian (1988) and that $\left|\boldsymbol{V}_{ag}^{\perp}\right| > 5$ m s^{-1} as well as $\left|\boldsymbol{V}_{g}\right| > 10$ m s^{-1}).
2. Dot-contoured areas, where the criterion (2) on the Rossby number is fullfilled in a region where the ageostrophic winds are significantly unbalanced

Figures 10 and 11 show that at 0000 UTC of 21/10 an area of significant unbalanced winds appears around 43.5° N. It widens, moves easterly becoming centered just upwind the station TRI_VAL when the event starts at 05000 UTC and weakens after 0800 UTC. The Rossby number is everywhere lower than 0.5 until 1200 UTC, when a small area with $Ro > 0.5$ appears at south-east. The analysis of the flow unbalancement based on the Rossby number shows therefore that this happened only in a small area and after the event.

5 | SHEAR INSTABILITY AND DISCUSSION

The coincidence of the MGW event with the alignement of the wind velocity at the wave direction and the increase of the wind at velocities slightly greater than the wave phase speed at the top of the troposphere suggests the hypothesis of wave generation by shear instability. By the way, Mastrantonio et al. (1976) showed that tropospheric jet streams can be a source for gravity waves with wavelenghts of the order of ten as well as a few hundred kilometers. The hypothesis of wave generation by shear instability is tested against linear-theory predictions in the following.

A linear stability analysis of the atmospheric flow around 0745 UTC 21 October (between maximum and minimum values of pressure fluctuations at TRI_VAL (Fig. 7) occurred at 0725 and 0800 UTC, respectively) has been performed following the technique described by Canavero et al. (1990). The linearization is based on the assumption that each atmospheric variable a can be expanded as $a(x, z, t) = \overline{a}(z) + a'(x, z, t)$ where x is the coordinate in the direction of wave propagation, z is the vertical coordinate positive upwards, $\overline{a}(z)$ is a background term and

$$a'(x, z, t) = Re(A'(z)e^{i(\omega t - k_x x)})$$

is the sinusoidal perturbation due to the wave. $Re()$ indicates the real part of a complex number, $i = (-1)^{1/2}$, $\omega = \omega_r + i\omega_i$ is the complex frequency, $k_x = 2\pi/\lambda$ is the real horizontal wavenumber and λ is the wavelength. The complex quantity $A'(z) = A_a(z)e^{i\phi_a(z)}$ represents the vertical structure of the wave and $A_a(z)$ and $\phi_a(z)$ are its amplitude and phase, respectively. The background state of the atmosphere is specified by the temperature $\overline{T}(z)$ and the wind speed $\overline{u}(z)$ along the direction of the wave propagation. The equations of motion and state for a dry atmosphere are used, ending in a system of four equations for the perturbations of horizontal and vertical wind components (u' and w', respectively),

pressure (p') and density (ρ'). It is convenient to introduce an auxiliary variable $D'(z)$, whose time derivative is essentially the vertical velocity, defined as ($W'(z) = i\Omega\epsilon D'(z)$), where $\Omega = \omega - k_x\overline{u}$ and $\epsilon = exp\int^z g/\overline{c}^2(z')dz'$. The variable $\overline{c} = (\gamma R\overline{T})^{1/2}$ is the speed of sound in air, R is the gas constant for dry air and $\gamma = c_p/c_v$ is the ratio of specific heats at constant pressure and volume, respectively. Using these new variables the system of four equations reduces to a single second-order ordinary differential equation (Chimonas (1970))

$$\frac{d}{dz}\left(\frac{r\Omega^2/k_x^2}{1-\Omega^2/(k_x^2\overline{c}^2)}\frac{dD'}{dz}\right) + r\,(N^2-\Omega^2)\,D' = 0 \tag{3}$$

where $r = \overline{\rho}\epsilon^2$, and $N^2 = -g[\overline{\rho}^{-1}d\overline{\rho}/dz + g/\overline{c}^2]$ is the square of the Brunt-Väisäla frequency. The problem is now reduced to numerically solving this equation for an atmosphere whose background state is specified by the known quantities $\overline{u}(z)$, $\overline{T}(z)$ and $\overline{\rho}$. The solution requires finding the eigenvalues ω and k_x and the associated eigenfunction $D'(z)$ with a boundary condition ($w' = 0$) at ground and a radiation condition at large heights ($w'(z)$ matching the analytical solution, which is known if both $\overline{u}(z)$ and $\overline{T}(z)$ constant). The eigenvalues are found using the shooting method of Lalas and Einaudi (1976). It consists in making an initial guess for the eigenvalues and a subsequent integration of the equation along z from the known value of D' at the top z_t of the integration domain to its value at $z = 0$ using the method of Burlisch and Stoer (1966). If the solution does not satisfy the boundary condition at ground the entire process is repeated varying the eigenvalues slightly until a convergence toward the correct solution is obtained. The amplitude and phase profiles of all the wave-induced perturbations can then be derived from $D'(z)$. The perturbations have been normalized by matching the amplitude of pressure perturbation at the ground with the value measured by the microbarometer at TRI_VAL.

The method employed in this study to determine the mean profiles follows very closely the procedure used by Canavero et al. (1990) and Koch et al. (1993). Functional fits to vertical profiles of background temperature $\overline{T}(z)$ and wind-velocity component along the direction of propagation $\overline{u}(z)$ were created through the linear combination of hyperbolic tangent and Gaussian functions to fit the sounding data in a least-squares sense and force a constant, uniform wind layer at the top of the integration domain in order to impose the radiation boundary condition. The Milano (MIL) sounding at 0006 UTC 21 Oct 1999 and wind-profiler-derived winds at approximately 0800 UTC, i.e., in the middle of the event, have been used. Temperature and velocity profiles, as well as the profiles of the Brunt-Väisälä frequency N^2 and the Richardson number Ri calculated from the fitted profiles are shown in Fig. 12. The N^2 profile shows that above the 2-km deep, very stable layer near the ground, the atmospheric stability progressively decreases up to the level where the Richardson number first decreases to below 0.25 (a necessary condition for dynamical instability). The Richardson number decreases to below 0.25 at 8.5 km and 11.5 km (straddling the jet maximum); at these heights the velocity is close to the phase speed of the wave measured at TRI , suggesting the possible existence of two critical levels.

The stability analysis showed that Eq. 3 , nondimensionalized using $H = 9$ km and $V = 30$ m s^{-1} as length and velocity scales respectively, is characterized by a family of unstable solutions in a wide range (0.511-0.861) of normalized wavenumber $\alpha = k_xH$. Their phase velocity ω_r/k_x and growth rate $-\omega_i$ are shown in Fig 13 as a function of the wavelength λ. The range of phase velocities is very narrow (26.913 m s^{-1} – 26.924 m s^{-1}), indicating that the system has little dispersion. Lack of dispersion tends to favor wind shear as the wave source (Koch and Dorian (1988),Gossard and Hooke (1975)). The phase velocity around 26.9 m s^{-1} is in good agreement with the measured value of 25 ± 3 m s^{-1}.

Looking at the fitted profile of the wind velocity component along the direction of propagation of the wave (Fig 12), the critical value of 26.9 m s^{-1} is reached at the heights of 8.5 km and 10.3 km, thus confirming the existence of two critical levels. The lowest falls inside the 340 m layer where $Ri < 0.25$ that is centred around 8.5 km, whereas the highest occurs just outside (40 m below) the 450 m layer where $Ri < 0.25$ that is centred around 10.6 km.

The reference mode with $\alpha_{ref} = 0.531$, i.e. wavelength of 106 km, has been chosen as the one whose value of $\alpha c_r = 2\pi H/(V\tau)$ matches the value $\tau = 66$ min of the pressure fluctuation period measured at TRI (c_r is the normalized phase speed). As in Canavero et al. (1990) and Koch et al. (1993) the reference mode does not correspond to a maximum of the growth rate, and the wave growth rate is very low, about 100 times lower than in the two cases analyzed by Koch et al. (1993). This is not unusual in atmospheric flows since the excitation of a particular mode may depend on a number of factors difficult to assess, such as horizontal inhomogeneities (at the longitude of the TRI_VAL station the distance between the Alps ridge at north and the Apennines ridge at south, i.e. the valley width above 0.5 km height, is equal to about two wavelenghts) , time variations of the background state, orography, turbulence structure and so on. Indeed, the stability analysis should not necessarily be viewed as a predictor for the observed wave-length, but rather as a means of obtaining the height variation and the relationships among the wave variables for a wave of the observed wavelength (Canavero et al. (1990)).

The amplitude and phase profiles of the perturbation pressure, temperature, horizontal and vertical velocities of the reference mode are shown in Fig 14. Also the other unstable modes of Fig 13 have essentially the same vertical structure. Below the critical level at 8.5 km height, the wave is characterized by a lack of any tilt and a series of constant-phase layers with subsequent phase reversals, the signature of a ducted wave that, in a 8.5 km duct, propagates horizontally with a standing pattern along the vertical. Above the critical level at 11 km the phases of all the variables increase linearly with the height, indicating vertical propagation. Following Lindzen and Tung (1976), the existence of a duct has always been supposed to explain the MGWs survival for many cycles. The ducted mode predicted by the stability analysis proves not only that in this event a duct exists, but also that it can be so deep to encompass almost the entire troposphere.

Even though Eq. 3 was derived for a compressible atmosphere and the linear stability analysis performed by Koch et al. (1993) was conducted using the incompressibility hypothesis, many features of the amplitude and phase profiles predicted by the present analysis agree with the analogous results regarding the unstable primary wave mode described by Koch et al. (1993): 1) below the lowest critical level there is a lack of wave tilt and a confinement of most of the wave amplitude, i.e. the ducting; 2) the pressure amplitude function displays a rapid decrease with height near the ground; 3) both horizontal wind and temperature amplitudes show large spikes and the vertical wind is negligible near the critical levels; 4) near the ground the horizontal and vertical winds are in quadrature and the horizontal wind and pressure perturbations are in phase (as sketched in Fig 15); 5) the horizontal wind perturbations reach their maximum amplitudes where the vertical wind perturbations have a node (and vice versa);

Fig 16 shows the vertical displacement, the (x,z) contour of the vertical-wind perturbation, the horizontal variation of the pressure perturbation at the ground predicted by the stability analysis and the rain rate at the ground displayed with the 14-min delay from the pressure perturbation. The horizontal variations of the vertical displacement and the vertical velocity below the first node at 3.5 km height is the same of that sketched in Fig 15. Also the pressure at the ground is in phase with the vertical displacement. On the other hand, the rain rate follows the pressure fluctuation, in contrast with the convective case assumed in Fig 15, where, in the absence of cloud physics considerations, the maximum cloudiness and rain rates should be expected at or just ahead of the wave ridge (Koch and Golus (1988)).

Fig 17 shows the vertical profile of the wave energy flux $F_E = \overline{p'w'}$ (Koch et al. (1993)), with the overbar representing an average over a wave period, compared with the temperature and the horizontal wind component profiles. It appears that at the height of 8.5 km, where the critical level is inside a layer with $Ri < 0$ and the instability develops, the energy flux is negative below and positive above, indicating that the energy flows away. Below the critical level the absolute value of the energy flux decreases approaching the ground: the wave extracts energy from the jet and distributes it inside the duct. This behaviour is quite different from that of Fig 10 in Koch et al. (1993), but similar to Fig 19 of Zhang et al. (2001).

As regards the consistency and the difference between the linear analysis prediction and the observations, Fig 18 shows the 55-75 min band-pass filtered temporal evolution of the vertical profiles of northward wind velocity component measured by the UHF windprofiler. A comparison with the vertical structure of the horizontal wind perturbation predicted by the stability analysis (Fig 14) indicates that the node at about 1.5 km height is clearly visible, while that at about 4.5 km seems to appear about 1 km below. Another comparison has been performed by calculating the lags that maximize the cross-correlation of UHF filtered signals at adjacent levels. The lags,after having been trasformed in terms of phases, are plotted in Fig 14, matched below 1,5 km height with the phase of the horizontal wind perturbation. Also the corresponding amplitudes have been plotted in Fig 14. Measured amplitudes result much greater than the predicted ones, but the 180° phase shift crossing the node at 1.5 km height is well captured, indicating a good agreement of the phase (the 2-min sampling rate implies a 11° uncertainty in phase detection).

Globally, Fig 18 and Fig 14 indicate that the results of the stability analysis agree with the UHF measurements in a satisfactory way. Much more difficult is the comparison of the delay between the rain rate and pressure fluctuation signals, due to the existence of layers of different depth, laid one over the other, where the perturbed quantities have opposite phases. Moreover, in contrast with the simpler case of Fig 15, where it is assumed that in a convective case the precipitation occurs just behind the maximum updraft and ahead of the change of sign of the wave-induced vertical-motion, in the present case the vertical motion could have influenced not only the condensation rate but also the fall speed of the hydrometeors, because a large fraction of the fall time was spent by the precipitation particles during their solid phase, i.e. at low fall speeds. The freezing level was in fact located at the 2.7 km height (Manfrin (2003)), with a melting layer at about 2 km height (Medina and Houze Jr (2003)). Also the drift action of horizontal motion cannot be neglected. In fact, even if the background wind does not modify the mean fall time, it influences the time lag. In the extreme case of a constant wind speed equal to the wave phase speed, the drifted precipitation particles have the same phase relationship with the wave during their fall (Richiardone and Manfrin (2003)). In this episode this effect was important because the wind velocity component along the direction of the wave propagation was everywhere greater than approximately two thirds of the wave speed between 2 km and 10 km height (Fig 12). A theoretical prediction of the lag between the rain and pressure fluctuations is therefore impossible without more complex modeling of the wave influence on precipitation microphysics.

Summarizing, the unstable mode predicted by the linear stability analysis agrees with the measurements and also with the current opinion that the wave must propagate in a duct. Unlike other trapped wave episodes (Koch et al. (1993), Trexler and Koch (2000)), in the present episode the duct encompassed almost the whole troposphere. The ducting, as a matter of fact, has been suggested in the literature as the mechanism that allows MGWs, whatever the process may be for its generation, to propagate at large distances without loosing their coherent structure because a duct is capped by a reflecting layer that limits the loss of wave energy. According to Lindzen and Tung (1976), the existence of a stable layer adjacent to the ground and capped by a sheared layer with $Ri < 0.25$ that contains a critical level is a condition favorable for a wave duct, provided that nowhere within the duct it exists an energy-absorbing level (i.e. a critical level where $Ri < 0.25$). Under these conditions (fulfilled in this episode, with the reflecting layer at 8.5 km height) a ducted mode can exist with little need for forcing. Even though the results of the linear stability analysis can be used strictly to describe only the initial stages of wave growth, linear theory often predicts well the main characteristics of the disturbances, that appear to persist past the linear stage. In practice, the wave growth caused by the instability is not observed because the wave quickly settles into steady-state behaviour brought about by nonlinear effects and/or dissipation (Canavero et al. (1990)). Even with these limitations, the linear prediction of the instability suggests that also in this episode, following Stobie et al. (1983) and Uccellini and Koch (1987), the shear layer at the duct top acted not only as a good reflector but as a resonator that feeds the wave extracting energy from the mean flow. Nevertheless, the synoptic setting and the presence of an area of unbalanced flow just upwind the measurements site and just at the

event start may not be casual. Therefore, even if the Rossby number never exceeded the value of 0.5 the hypothesis of a role of the geostrophic adjustment in the triggering of the instability or even selecting the mode cannot be excluded.

6 | CONCLUSIONS

Thanks to deployment of a sensitive high-precision pluviometer it has been confirmed that a wave can modulate the stratiform precipitation, a process that is has been more easily and frequently observed in convective-precipitation episodes.

The simultaneous increase of rain-rate and gravity-wave activity as well as the rain modulation that was observed during this event occurred at the end of a synoptic setting which is known as favorable for the generation of mesoscale gravity waves by geostrophic adjustment of an unbalanced flow. The analysis of the flow unbalancement based on the Rossby number has however shown that this happened only in a small area and after the event.

The linear stability analysis, on the contrary, showed that an unstable and ducted mesoscale-wave mode of about 100 km wavelenght originating from the shear instability of the tropospheric jet and in agreement with the measurements could exist, but it cannot be excluded that the a partially unbalanced flow, as well as topography, may have played a role.

This supports the current hypothesis that mesoscale gravity waves can survive for many cycles thanks to the existence of a duct that in this case is 8.5 km height, the deepest ever observed. The analysis of this event also supports the hypothesis that a critical level (a level where the unperturbed flow speed is equal to the phase speed of the wave) in a sheared layer not only creates a duct, but can also serve as a generation mechanism for the mesoscale gravity waves, provided that the local shear is sufficiently strong that $Ri < 0.25$. In fact, as it has been pointed by some authors, the critical level should not be viewed only as a guiding mechanism which prevents leakage of wave energy upward, but also as a region where the wave will continue to extract kinetic energy from the basic state along its entire track.

ACKNOWLEDGEMENTS

The authors wish to thank D. Bertoni for the setting of the microbarometer network, E. Curiotto for his thesis work, A. Guarise and other two anonymous students for the patience shown in calibrating the pluviometer and R. Rotunno for his helpful comments and suggestions.

REFERENCES

Bosart, L. and Seimon, A. (1988) A study of an unusually intense atmospheric gravity wave. *Mon. Wea. Rev.*, 1857–1886.

Bougeault, P., Binder, P., Buzzi, A., Dirks, R., Houze, R., Kuettner, J., Smith, R., Steinacker, R. and Volkert, H. (2001) The MAP Special Observing Period. *Bull. Am. Meteorol. Soc.*, 433–462.

Bousquet, O. and Smull, B. F. (2003) Observations and impacts of upstream blocking during a widespread orographic precipitation event. *Q. J. R. Meteorol. Soc.*, 391–409.

Burlisch, R. and Stoer, J. (1966) Numerical treatment of ordinary differential equations by extrapolation methods. *Num. Math.*, 1–13.

Canavero, F. G., Einaudi, F., WestWater, E. R., Falls, M. J., Schroeder, J. A. and Bedard Jr., A. J. (1990) Interpretation of ground-based radiometric observations in terms of a gravity wave model. *J. Geophys. Res.*, 7637–7652.

Chimonas, G. (1970) The extension of the Miles-Howard theorem to compressible fluids. *J. Fluid Mech.*, 833–836.

DeMaria, M., Davis, J. M. and M., W. D. (1989) Observations of mesoscale wave disturbances during the genesis of atlantic lows experiment. *Mon. Wea. Rev.*, 826–842.

Einaudi, F., Bedard Jr., A. J. and Finnigan, J. J. (1989) A climatology of gravity waves and other coherent disturbances at the Boulder atmospheric observatory during march-april 1984. *J. Atmos. Sci.*, 303–329.

Ferretti, R., Einaudi, F. and Uccellini, L. W. (1988) Wave disturbances associated with the Red River valley severe outbreak of 10-11 April 1979. *Meteorol. Atmos. Phys.*, 132–168.

Ford, R., McIntyre, M. E. and Norton, W. A. (2000) Balance and the slow quasimanifold: Some explicit results. *J. Atmos. Sci.*, 1236–1254.

Gossard, E. E. and Hooke, W. H. (1975) *Waves in the Atmosphere. Developments in Atmospheric Science, 2*. Elsevier Scientific.

Grivet-Talocia, S., Einaudi, F., Clark, W. L., Dennett, R. D., Nastrom, G. D. and VanZandt, T. E. (1999) A 4-yr climatology of pressure disturbances using a barometer network in central Illinois. *Mon. Wea. Rev.*, 1613–1629.

Houser, J. L. and Bluestein, H. B. (2011) Polarimetric doppler radar observations of Kelvin-Helmholtz waves in a winter storm. *J. Atmos. Sci.*, 1676–1702.

Jewitt, B. F., Ramamurthy, M. K. and Rauber, R. M. (2003) Origin, evolution, and finescale structure of the St. Valentine's day mesoscale gravity wave observed during STORM-FEST. part III: Gravity wave genesis and the role of evaporation. *Mon. Wea. Rev.*, 617–633.

Jiang, Q. and Doyle, J. D. (2004) Gravity wave breaking over the Central Alps: Role of complex terrain. *J. Atmos. Sci.*, 2249–2266.

Kaplan, M. L., Koch, S. E., Lin, Y., Weglarz, R. P. and Rozumalski, R. A. (1997) Numerical simulations of a gravity wave event over CCOPE, part I: The role of geostrophic adjustment in mesoscale jetlet formation. *Mon. Wea. Rev.*, 1185–1211.

Keil, C. and Cardinali, C. (2004) The ECMWF reanalysis of the MAP special observing period. *Q.J.R. Meteorol. Soc.*, 2827–2849.

Koch, S. E. and Dorian, P. B. (1988) A mesoscale gravity wave event observed during CCOPE. part III: Wave environment and probable source mechanisms. *Mon. Wea. Rev.*, 2570–2592.

Koch, S. E., Einaudi, F., Dorian, P. B.and Lang, S. and Heymsfield, G. M. (1993) A mesoscale gravity wave event observed during CCOPE, part IV: Stability analysis and doppler-derived wave vertical structure. *Mon. Wea. Rev.*, 2483–2510.

Koch, S. E. and Golus, R. E. (1988) A mesoscale gravity wave event observed during CCOPE, part I: Multiscale statistical analysis of wave characteristics. *Mon. Wea. Rev.*, 2527–2544.

Koch, S. E., Golus, R. E. and Dorian, P. B. (1988) A mesoscale gravity wave event observed during CCOPE, part II: Interactions between mesoscale convective systems and the antecedent waves. *Mon. Wea. Rev.*, 2545–2569.

Koch, S. E. and O'Handley, C. (1997) Operational forecasting and detection of mesoscale gravity waves. *Wea. Forecasting*, 253–281.

Koch, S. E. and Siedlarz, L. M. (1999) Mesoscale gravity waves and their environment in the central United States during STORM-FEST. *Mon. Wea. Rev.*, 2854–2879.

Lalas, D. P. and Einaudi, F. (1976) On the characteristics of gravity waves generated by atmospheric shear layers. *J. Atmos. Sc.*, 1248–1259.

Lindzen, R. S. and Tung, K. K. (1976) Banded convective activity and ducted gravity waves. *Mon. Wea. Rev.*, 1602–1617.

Manfrin, M. (2003) Meccanismi di generazione di onde di gravità atmosferiche e loro interazione con il mare e le precipitazioni. *Ph. Thesis of the Università degli Studi di Genova (in italian)*, 1–145.

Mastrantonio, G., Einaudi, F., Fua, D. and Lalas, D. P. (1976) Generation of gravity waves by jet streams in the atmosphere. *J. Atmos. Sci.*, 1730–1738.

Medina, S. and Houze Jr, R. A. (2003) Air motions and precipitation growth in Alpine storms. *Q.J.R. Meteorol. Soc.*, 345–371.

O'Sullivan, D. and Dunkerton, T. J. (1995) Generation of inertia-gravity waves in a simulated life cycle of baroclinic instability. *J. Atmos. Sci.*, 3695–3716.

Palmén, E. and Newton, C. W. (1969) Atmospheric circulation systems. 606 pp. , Academic Press.

Plougonven, R. and Snyder, C. (2007) Inertia-gravity waves spontaneously generated by jets and fronts. part I: Different baroclinic life cycles. *J. Atmos. Sci.*, 2502–2520.

Plougonven, R. and Zhang, F. (2014) Internal gravity waves from atmospheric jets and fronts. *Rev. Geophys.*, 1–37.

Powers, J. G. and Reed, R. J. (1993) Numerical simulation of the large-amplitude mesoscale gravity-wave event of 15 december 1987 in the Central United States. *Mon. Wea. Rev.*, 2285–2308.

Ralph, F. M., Crochet, M. and Venkateswaran, S. V. (1993) Observations of a mesoscale ducted gravity wave. *J. Atmos. Sci.*, 3277–3291.

Richiardone, R. (1993) The transfer function of a differential microbarometer. *J. Atmos. Oceanic Technol.*, 624–628.

Richiardone, R. and Manfrin, M. (2003) A rain episode related to a mesoscale gravity wave. *Bull. Am. Meteorol. Soc.*, 1494–1498.

Richiardone, R., Manfrin, M. and Curiotto, E. (2001) Gravity waves detection from microbarometric measurements in the western Po valley. *MAP newsletter, 15*, 43–46.

Rotunno, R. and Houze, R. (2007) Lesson on orographic precipitation from the Mesoscale Alpine Programme. *Q.J.R. Meteorol. Soc.*, 811–830.

Ruppert Jr, J. H. and Bosart, L. F. (2014) A case study of the interaction of a mesoscale gravity wave with a mesoscale convective system. *Mon. Wea. Rev.*, 1403–1429.

Saïd, F., Campistron, B., Delbarre, H., Canut, G., Doerenbecher, A., Durand, P., Fourrié, N., Lambert, D. and Legain, D. (2016) Offshore winds obtained from a network of wind profiler radars during HyMeX. *Q. J. R. Meteorol. Soc., special issue HYMEX*, 23–42.

Stobie, J. G., Einaudi, F. and Uccellini, L. W. (1983) A case study of gravity waves-convective storms interaction: 9 May 1979. *J. Atmos. Sci.*, 2804–2830.

Trexler, C. M. and Koch, S. E. (2000) The life cycle of a mesoscale gravity wave as observed by a network of doppler wind profilers. *Mon. Wea. Rev.*, 2423–2446.

Uccellini, L. W. and Koch, S. E. (1987) The synoptic setting and possible energy sources for mesoscale wave disturbances. *Mon. Wea. Rev.*, 721–729.

Volkert, H. and Gutermann, T. (2007) Inter-domain cooperation for mesoscale atmospheric laboratories: the Mesoscale Alpine Programme as a rich study case. *Q.J.R. Meteorol. Soc.*, 949–967.

Wang, S. and Zhang, F. (2010) Source of gravity waves within a vortex-dipole jet revealed by a linear model. *J. Atmos. Sci.*, 1438–1455.

Wei, J. and Zhang, F. (2014) Mesoscale gravity waves in moist baroclinic jet-front systems. *J. Atmos. Sci.*, 929–952.

Wu, L. J., Wen, Z. P. and He, H. Y. (2015) Relationship between the periodic fluctuations of pressure and precipitation during a rainstorm. *Atmos. Ocea. Sci. Let.*, 78–81.

Zhang, F. (2004) Generation of mesoscale gravity waves in upper-tropospheric jet-front systems. *J. Atmos. Sci.*, 440–457.

Zhang, F., Koch, S. E., Davis, C. A. and Kaplan, M. L. (2001) Wavelet analysis and the governing dynamics of a large-amplitude mesoscale gravity-wave event along the East Coast of the United States. *Q.J.R. Meteorol. Soc.*, 2209–2245.

Zhang, F., Zhang, M., Wei, J. and Wang, S. (2013) Month-long simulations of gravity waves over North America and North Atlantic in comparison with satellite observations. *Acta Meteor. Sinica*, 446–454.

Zülicke, C. and Peters, H. W. (2007) Impact of upper-level jet-generated inertia-gravity waves on surface wind and precipitation. *Atmos. Chem. Phys. Discuss.*, 15873–15909.

GRAPHICAL ABSTRACT

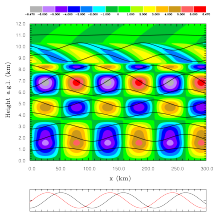

An episode of stratiform rain modulated by a Mesoscale Gravity Wave with a period of approximately 1 h and a 100-km wavelength is investigated. A two-dimensional linear stability analysis of the flow suggests the existence of an unstable mode originating from the shear instability of the tropospheric jet and propagating in a duct encompassing almost the entire troposphere. The results of the theoretical analysis are shown to be in good agreement with the measurements from a microbarometer network and wind-profiler soundings.

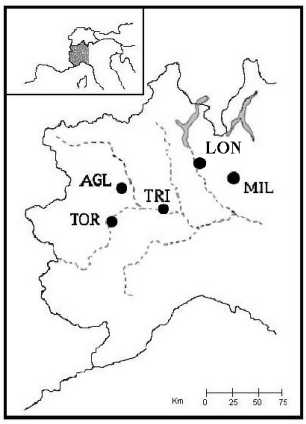

FIGURE 1 Map of the western part of the Po Valley (Italy) showing the placement of instruments: three-microbarometer array in Torino (TOR), one microbarometer in Agliè (AGL), three-microbarometer array in Trino Vercellese (TRI), VHF and UHF windprofilers in Lonate Pozzolo (LON) and radio soundings in Milano (MIL) (after Richiardone and Manfrin (2003))

.

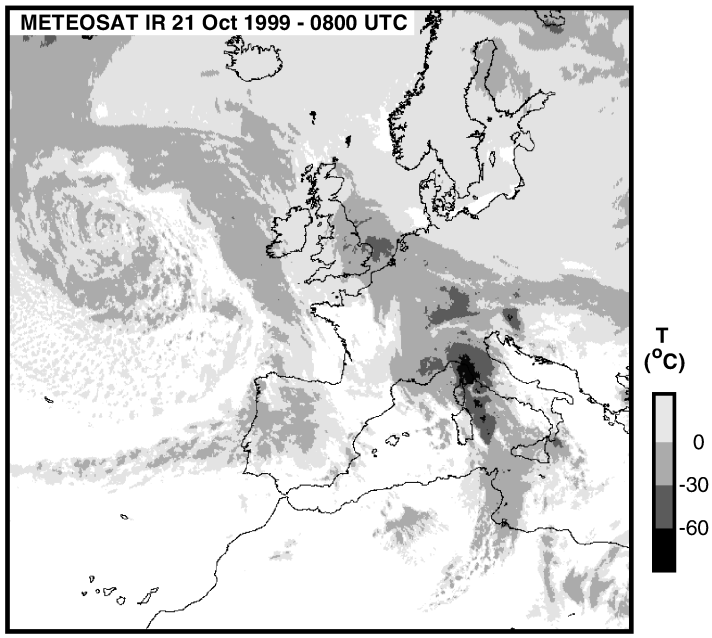

FIGURE 2 Meteosat infrared satellite image at 0800 UTC 21 October 1999. Shading indicates black-body temperatures (key at lower right), with black indicating temperatures $< -60\,^{\circ}\mathrm{C}$ atop active convection (after Bousquet and Smull (2003)).

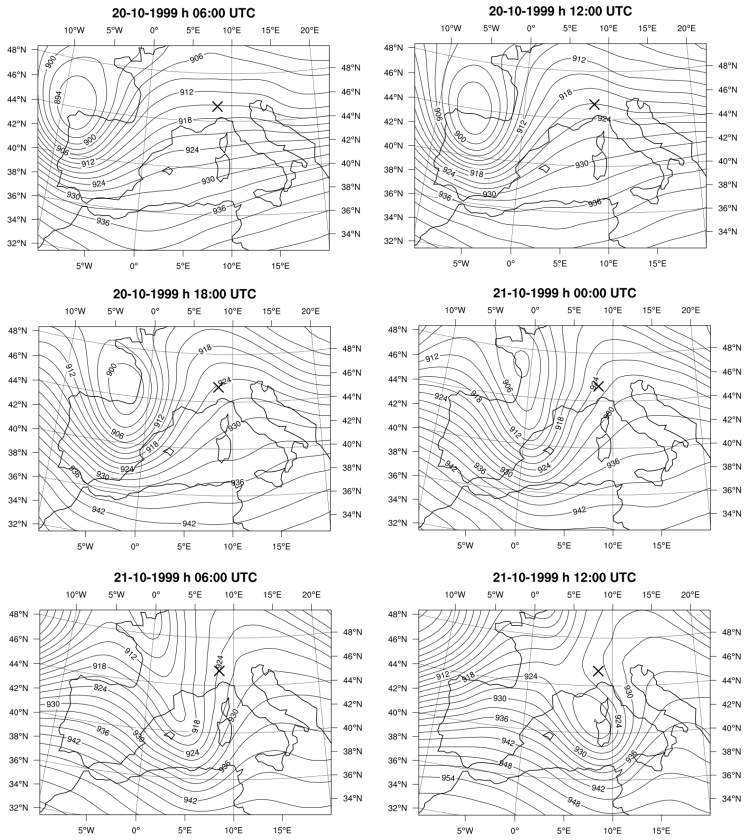

FIGURE 3 300 hPa geopotential height (dam) ECMWF analysis from 0600 UTC on 20 Oct 1999 to 1200 UTC on 21 Oct 1999. The cross shows the position of the TRI microbarometric network.

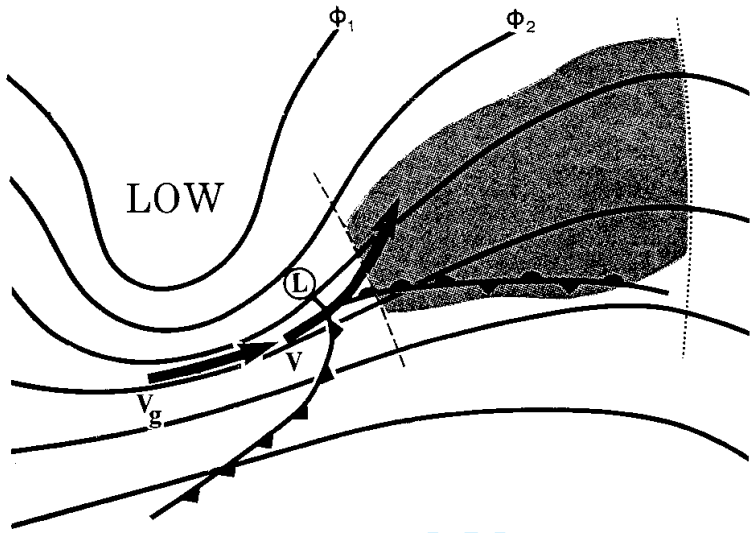

FIGURE 4 Schematic model from Uccellini and Koch (1987) delineating the region of greatest potential for gravity-wave occurrence (shaded) in the 300-hPa height field. Gravity waves are generated near the axis of inflection (dashed line) and decay upon approaching the ridge axis (dotted line). An upper-level jet streak (**V**) must be propagating toward the inflection axis, and away from the geostrophic wind maximum ($\mathbf{V}_g$) located at the base of the trough, for gravity waves to be generated by geostrophic adjustment processes (after Koch and O'Handley (1997)). ©American Meteorological Society. Used with permission

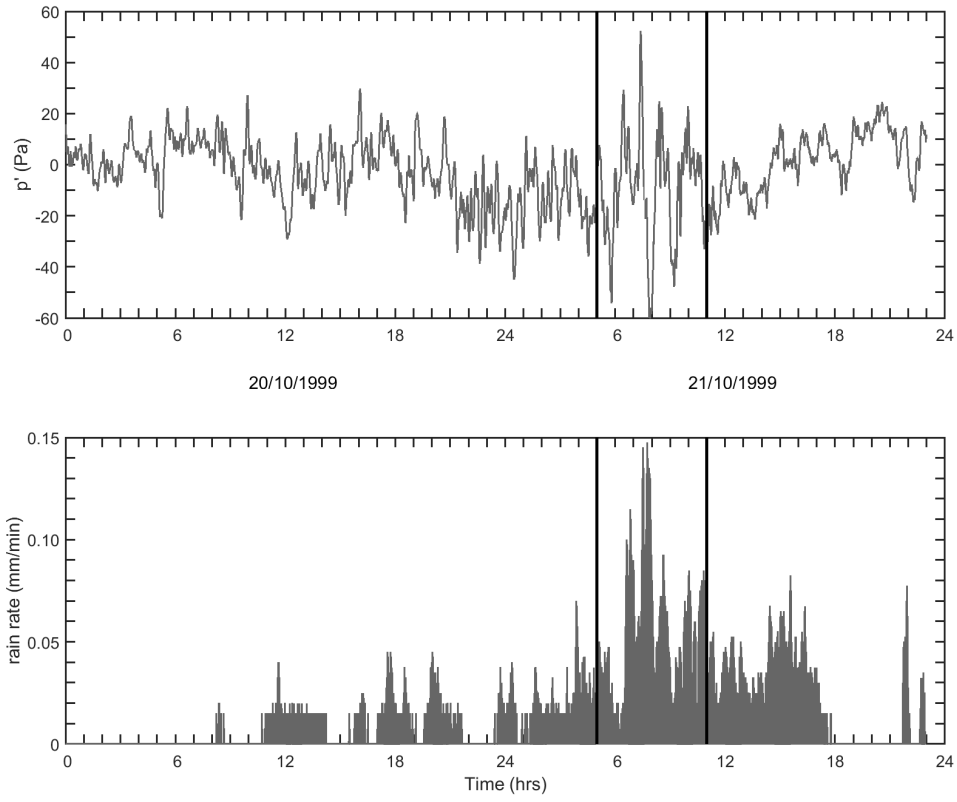

FIGURE 5 UTC-time series (raw data) of pressure fluctuations and rain rate at TRI_VAL station on 20 and 21 Oct 1999. Vertical bars bound the MGW-precipitation event.

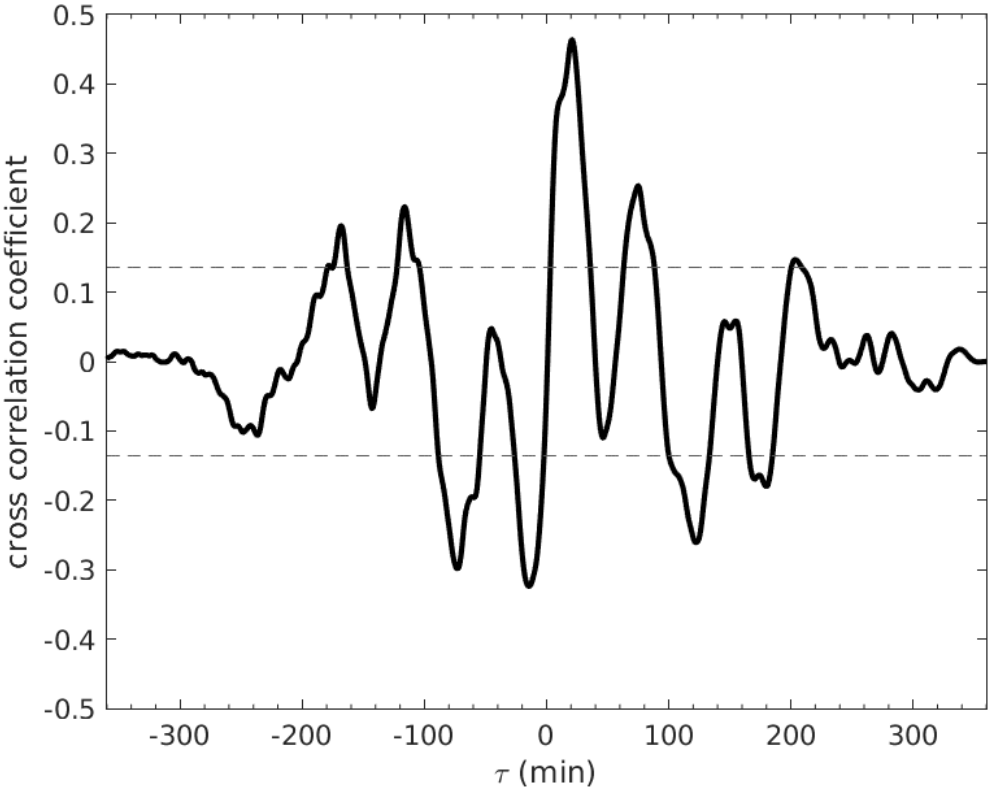

FIGURE 6 Cross-correlation coefficient between the raw signals of pressure fluctuations $p'(t)$ and rain rate $r(t+\tau)$ during the 6-h event. The dashed lines indicate the two-sided 1 % confidence limits.

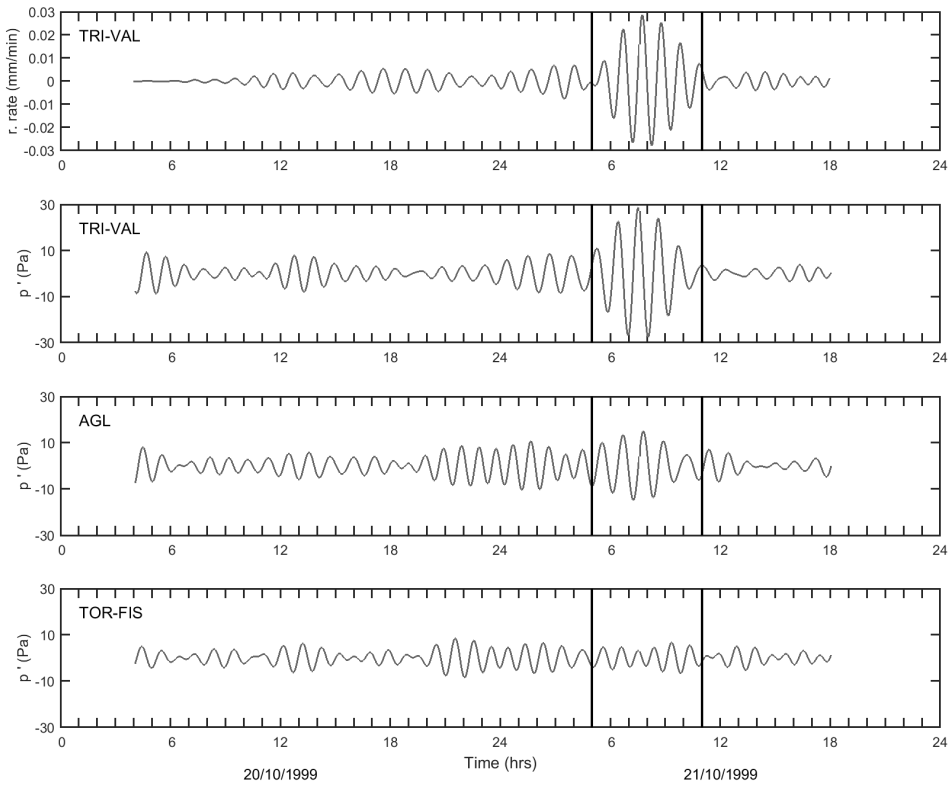

FIGURE 7 55 - 75 min band-pass-filtered rain rate and pressure at TRI_VAL, AGL and TOR_FIS on 20 and 21 Oct 1999. At both sides the data have been dropped to mask the band-pass side effects. Vertical bars bound the MGW-precipitation event.

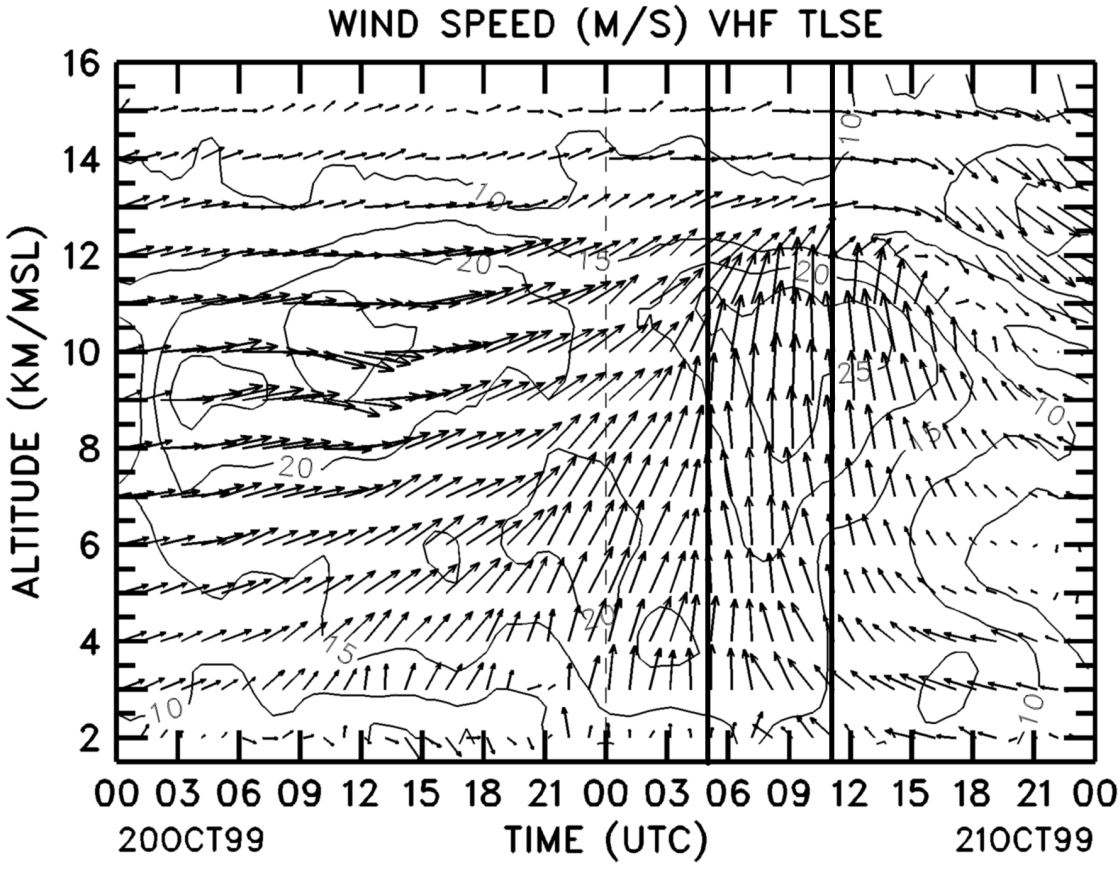

FIGURE 8 Temporal evolution of wind speed and direction vertical profiles from VHF windprofiler in Lonate Pozzolo. Wind speed contours in m s^{-1}. Vertical bars bound the MGW-precipitation event, highlighting the tropospheric jet transit at 10 km height simultaneously with southerly winds occurrence throughout the troposphere.

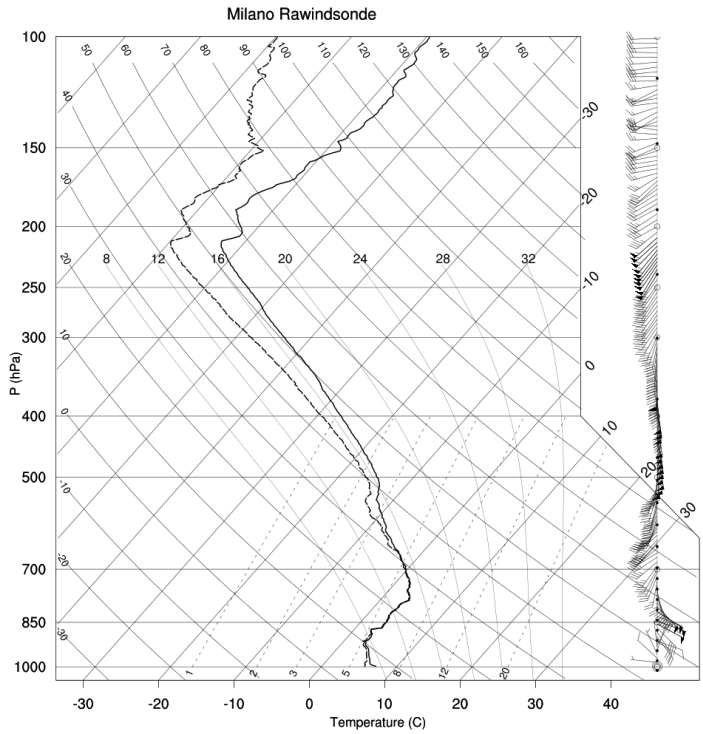

FIGURE 9 Milano (MIL) sounding at 0600 UTC on 21 Oct 1999: Skew T-log p diagram with temperature (continuous line), dew-point temperature (dashed line) and wind speed and direction.

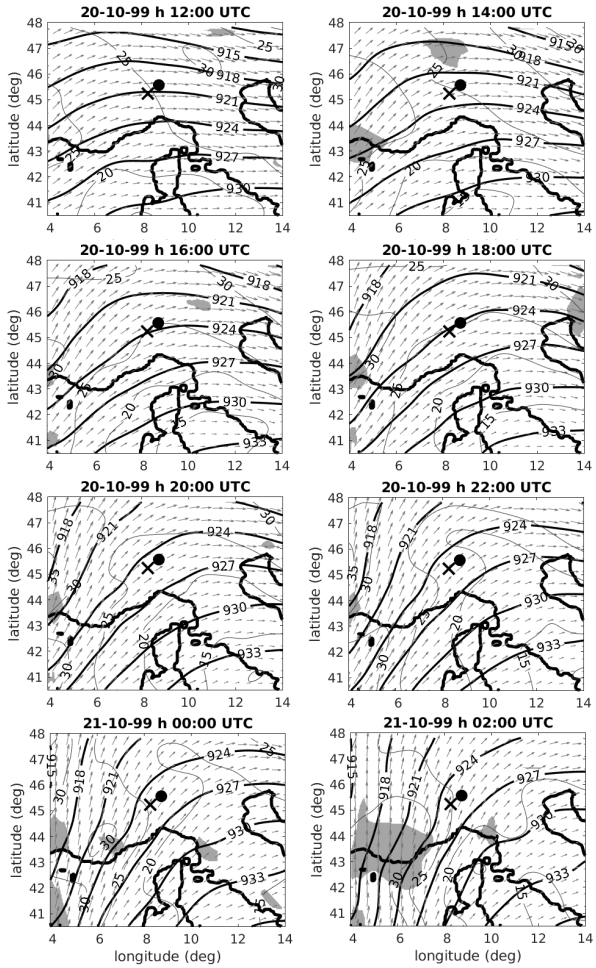

FIGURE 10 Geopotential heights contours (dam, heavy lines), wind speed contours (m s^{-1}, thin lines), wind velocity vectors and the regions of unbalanced flow from 1200 UTC of 20 October to 0200 UTC of 21 October. Stippled and heavy dot-contoured areas highlight the regions where unbalanced ageostrophic winds are significant and where $Ro > 0.5$, respectively. The cross and the bullet show the position of the TRI_VAL and LON stations, respectively.

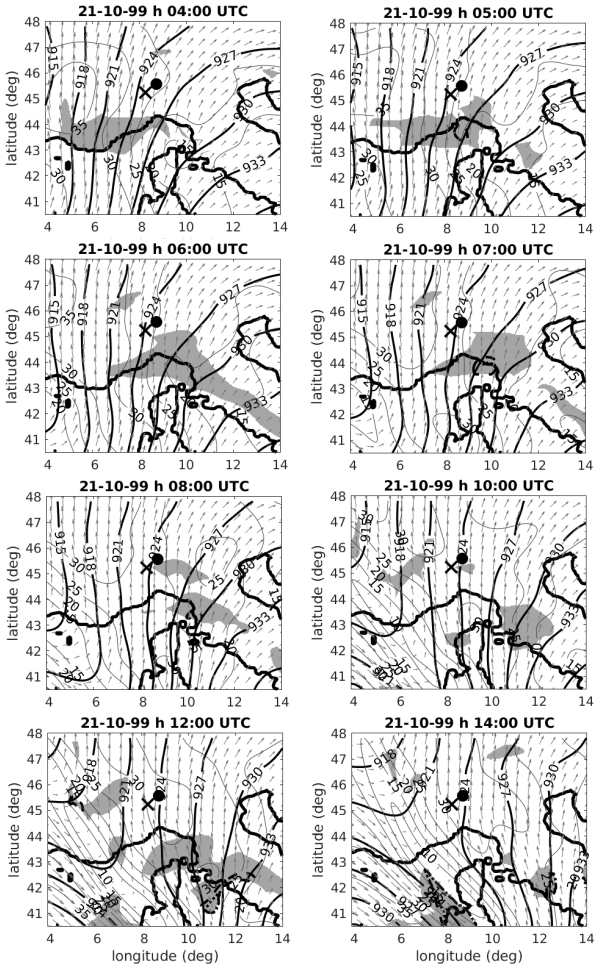

FIGURE 11 As Fig. 10, but from 0400 UTC to 1400 UTC of 21 October.

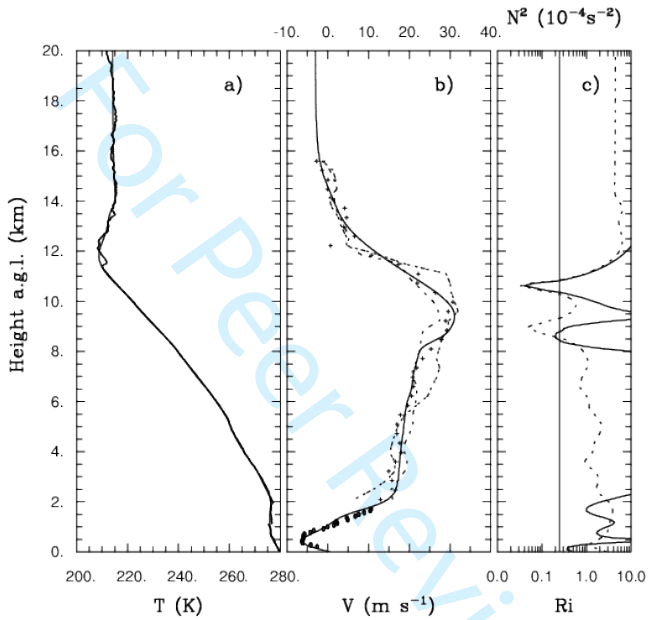

FIGURE 12 Temperature profile fit (continuous line) compared with Milano (MIL) sounding at 0600 UTC on 21 Oct 1999 (crosses) (a); Northward wind velocity component fit (continuous line) compared with VHF windprofiler sounding at 0717 UTC (dashed line), at 0746 UTC (crosses), at 0815 UTC (dot-dashed line) and, below 2 km, UHF windprofiler at 0742 UTC (circles) (b); Richardson number Ri (continuous line) and the square of Brunt-Väisälä frequency N^2 (dashed line) calculated from the fitted profiles, with the vertical dashed line indicating $Ri = 0.25$ (c).

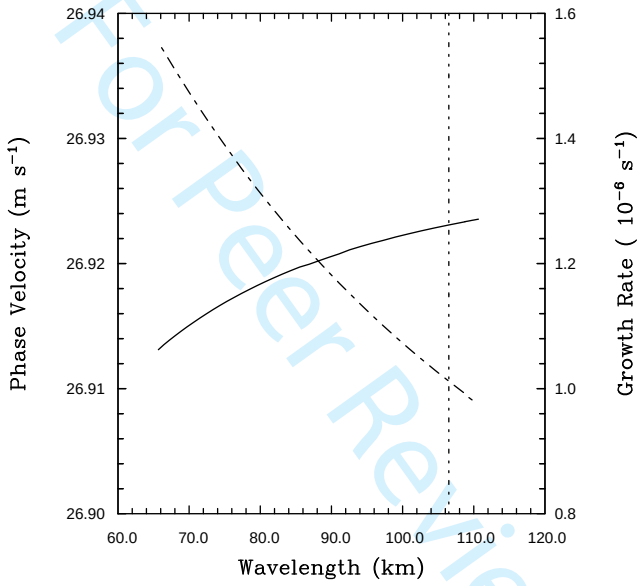

FIGURE 13 Phase velocity (continuous line) and growth rate (dot-dashed line) of the unstable solutions of Eq. (1) as a function of the wavelength. The vertical, dashed line indicates the reference mode, the one whose period matches the measured value of pressure fluctuations period at TRI.

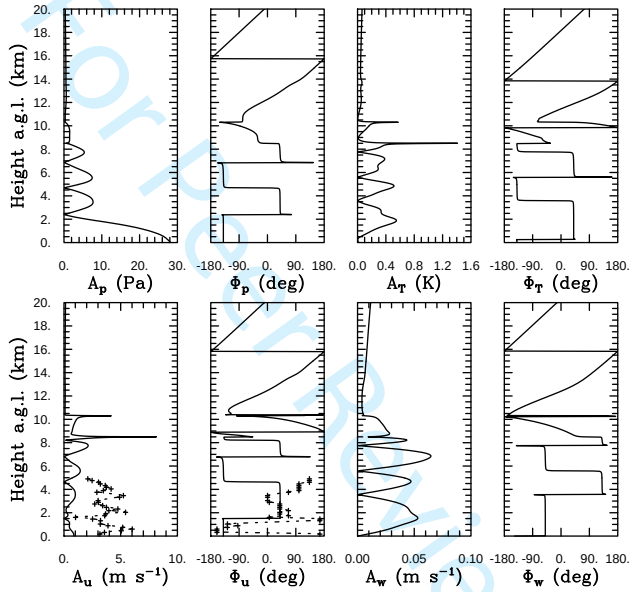

FIGURE 14 Linear analysis prediction of amplitude and phase profiles of perturbation pressure, temperature, horizontal- and vertical- wind components of the reference mode. The amplitude and phase of the horizontal-wind perturbation derived from the UHF windprofiler band-pass filtered measurements are indicated by the crosses.

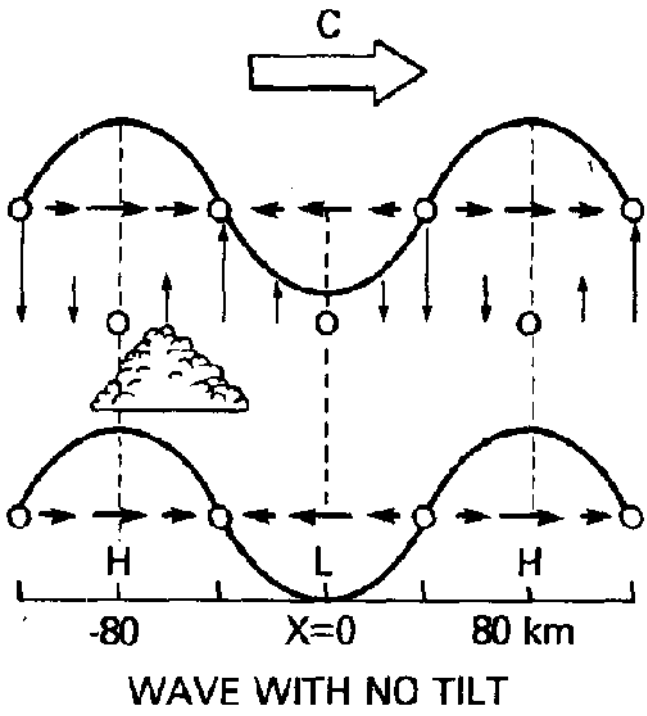

FIGURE 15 Schematic illustration of the height variation in the phase relations between the horizontal wind component in the direction of wave propagation and the wave-induced vertical motions for a ducted wave (wave with no tilt) in a convective case. Also shown is location of strongest convection relative to gravity wave crest, assumed to be $\pi/4$ behind maximum updraft. The wave propagates to the right with phase speed C. H and L refer to high and low pressure perturbations at the ground (after Koch and Golus (1988)). ©American Meteorological Society. Used with permission.

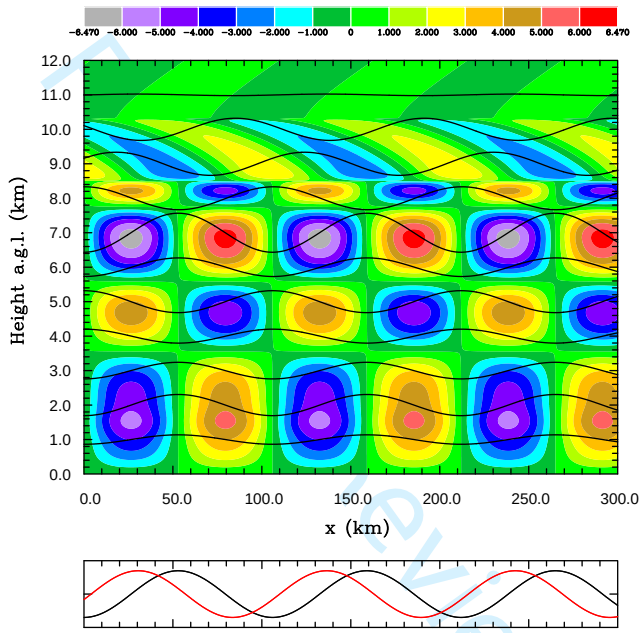

FIGURE 16 Stability analysis prediction: (x,z) contour of the vertical-wind perturbation (cm s^{-1}) and wave displacement (km, black lines) multiplied by 6 in 1 km height steps (top), pressure perturbation (black) and observed rain rate modulation (red) at ground in arbitrary units (bottom).

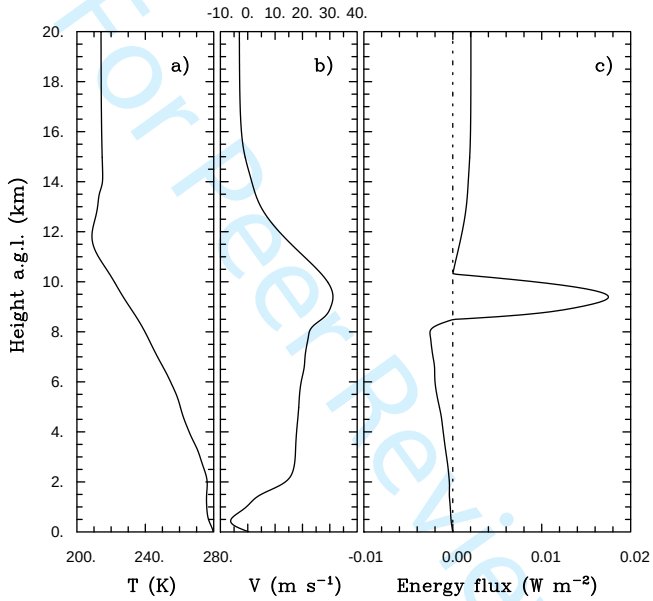

FIGURE 17 Temperature profile fit (a); Northward wind-velocity component fit (b); Wave energy flux (c).

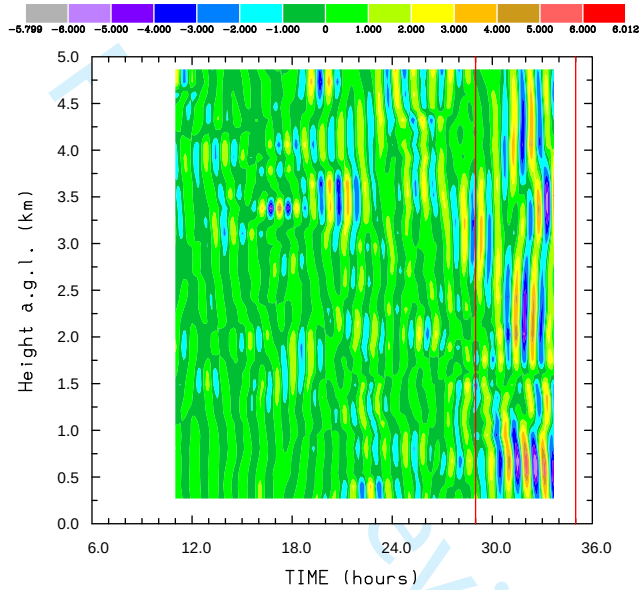

FIGURE 18 55 -75 min band-pass-filtered temporal evolution of the vertical profiles of northward wind-velocity component measured by the UHF wind profiler at Lonate Pozzolo from 0600 UTC of 20 Oct to 1200 UTC of 21 Oct 1999. Wind speed contouring in m s^{-1} . Red vertical bars bound the MGW-precipitation event. The data have been dropped on both sides to mask the band-pass side effects.

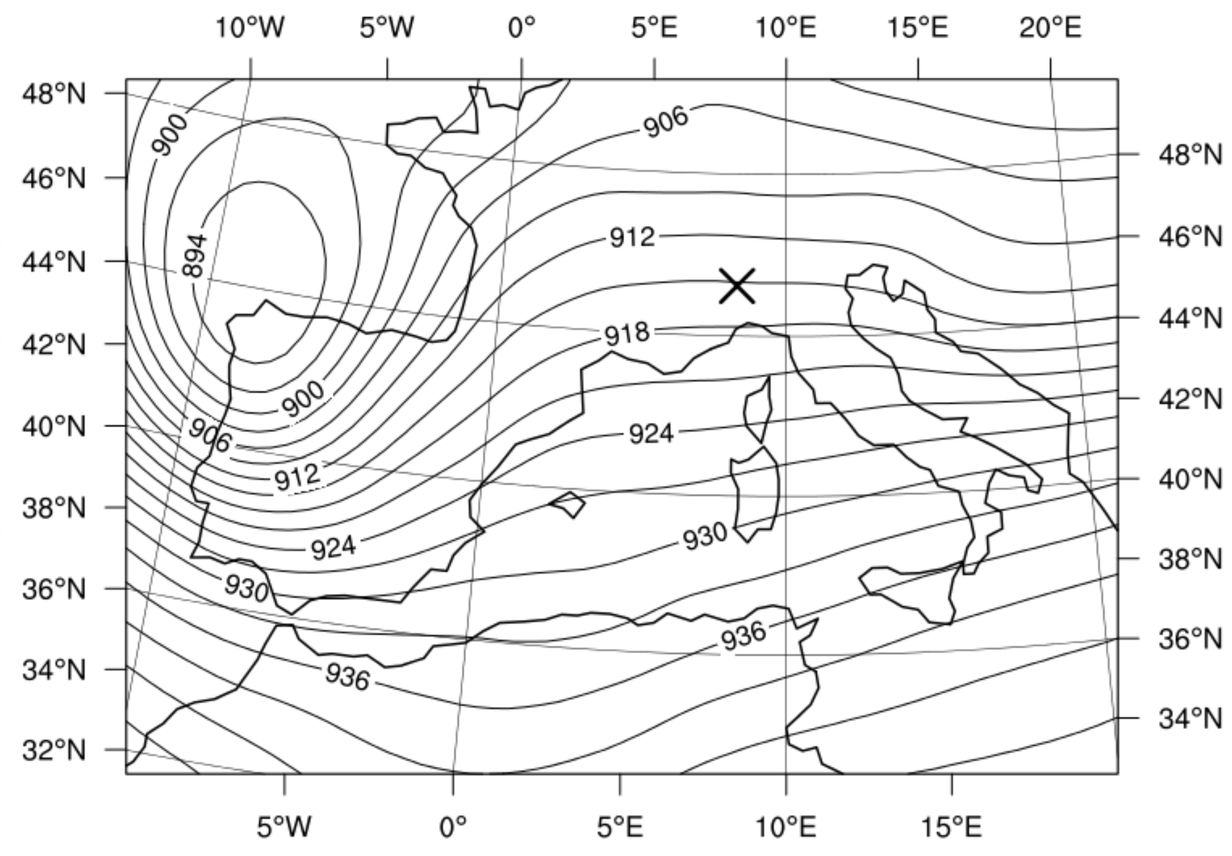
20-10-1999 h 06:00 UTC
10°W 5°W 0° 5°E 10°E 15°E 20°E
48°N 46°N 44°N 42°N 40°N 38°N 36°N 34°N 32°N
900 906 894 912 918 924 930 936

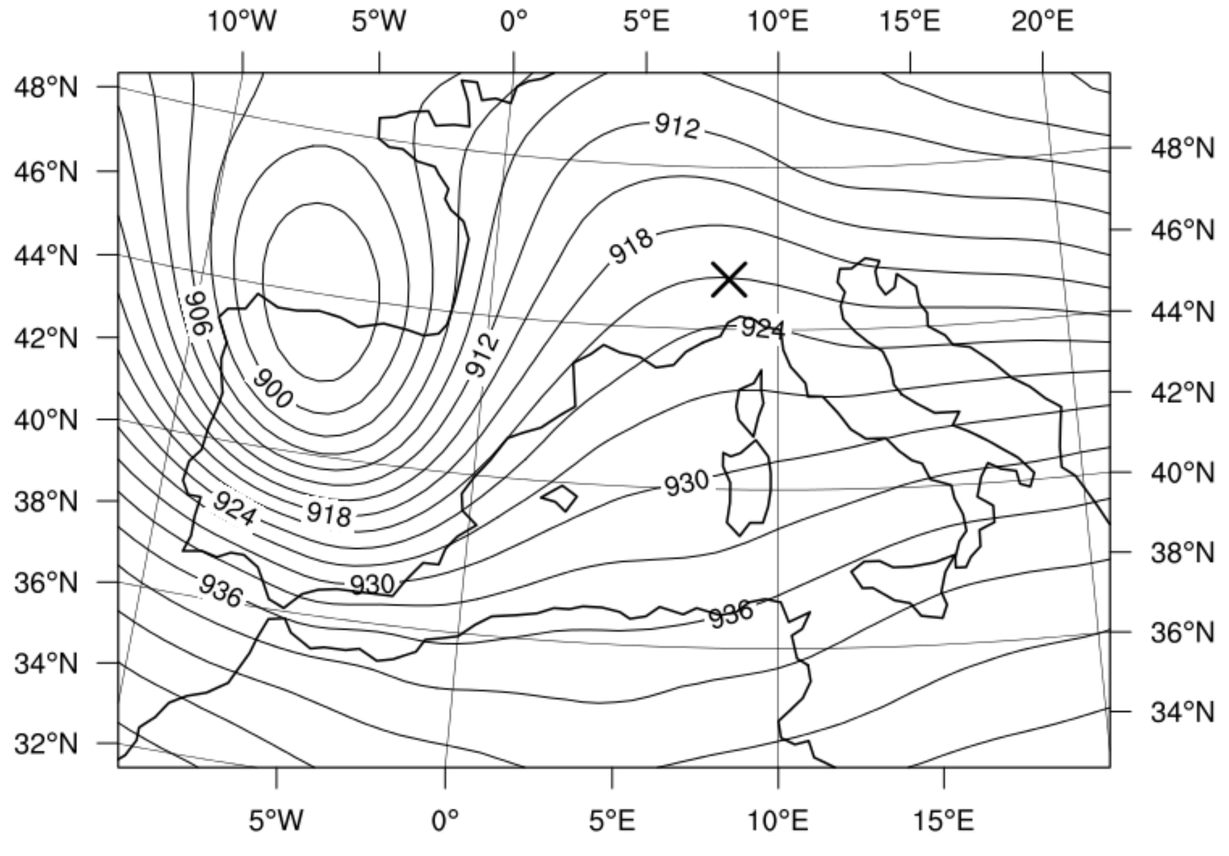
20-10-1999 h 12:00 UTC
10°W 5°W 0° 5°E 10°E 15°E 20°E
48°N 46°N 44°N 42°N 40°N 38°N 36°N 34°N 32°N
912 918 906 900 912 924 930 924 918 936 936

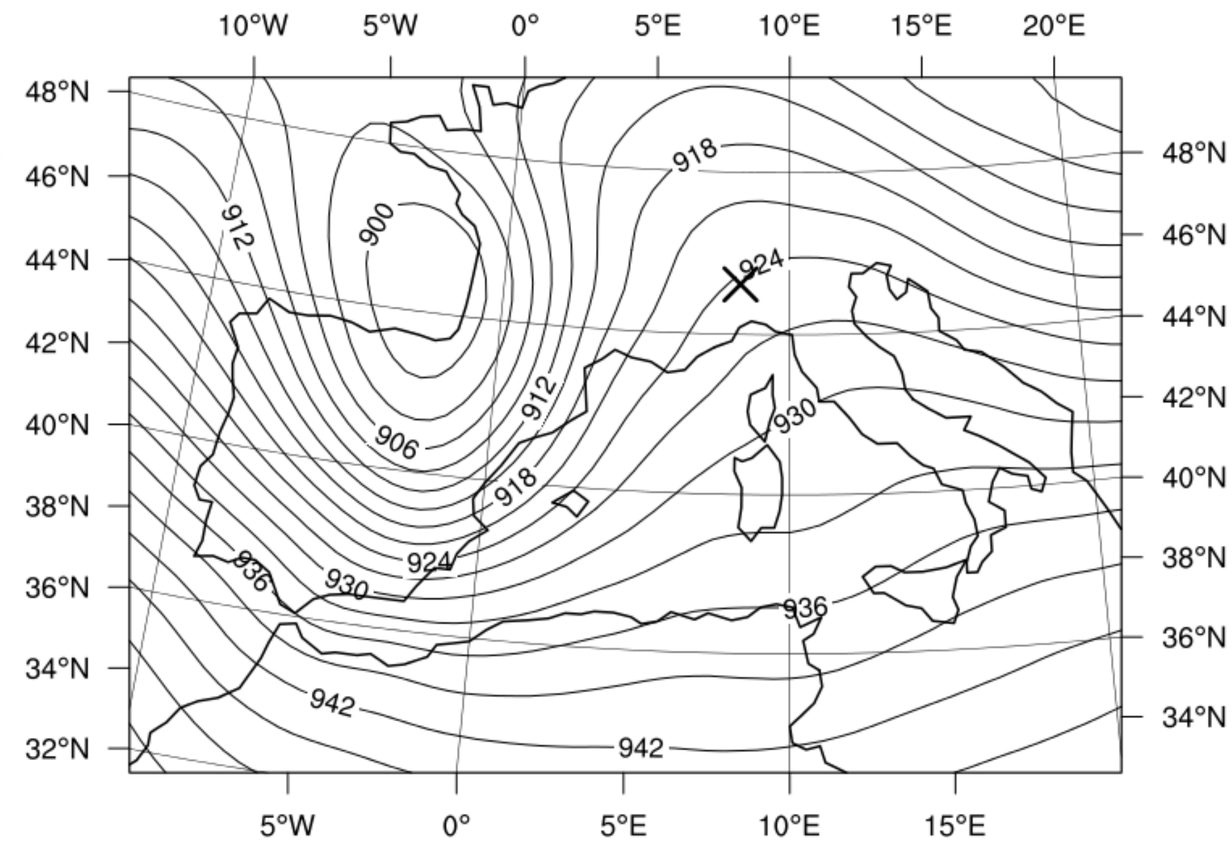
20-10-1999 h 18:00 UTC
10°W 5°W 0° 5°E 10°E 15°E 20°E
48°N 46°N 44°N 42°N 40°N 38°N 36°N 34°N 32°N
912 900 918 924 906 912 918 930 936 930 936 942 942

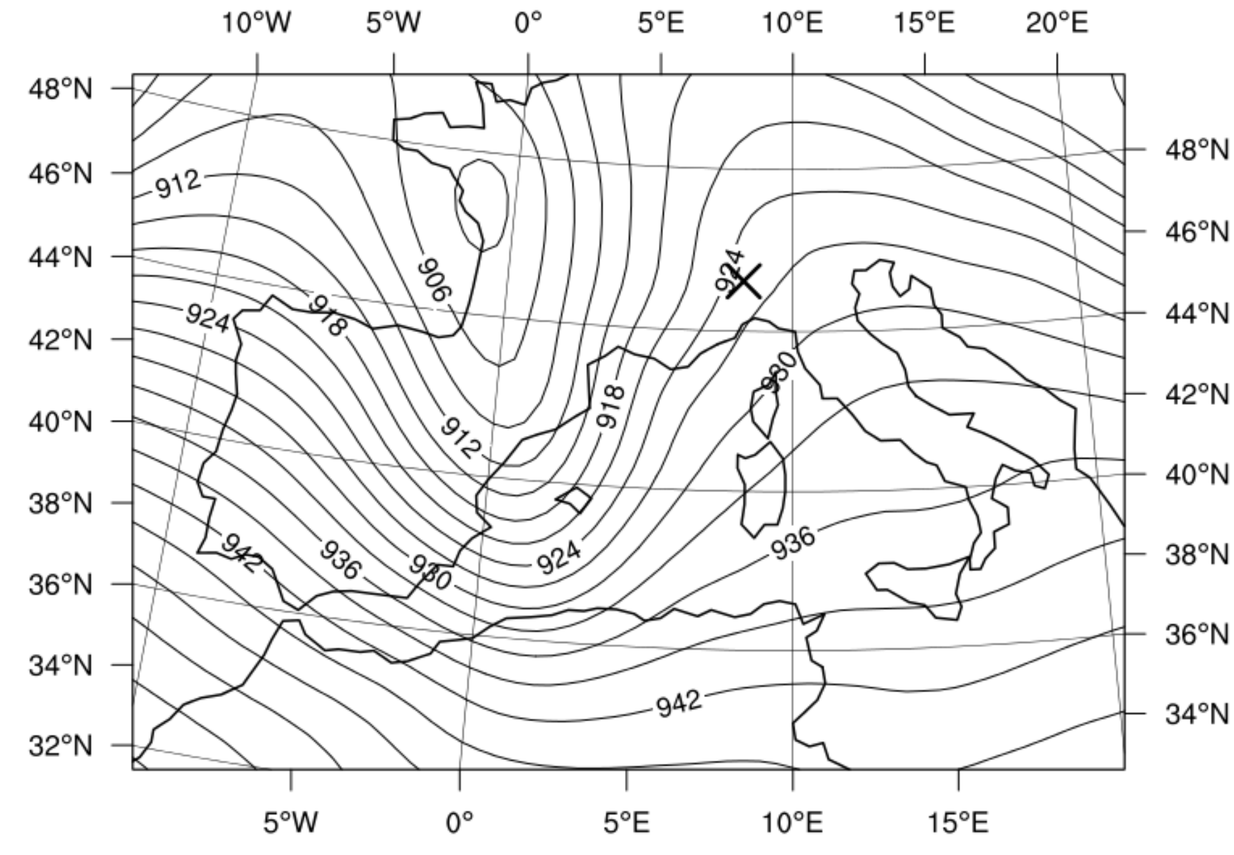
21-10-1999 h 00:00 UTC
10°W 5°W 0° 5°E 10°E 15°E 20°E
48°N 46°N 44°N 42°N 40°N 38°N 36°N 34°N 32°N
912 906 924 918 924 918 912 980 942 936 930 924 936 942

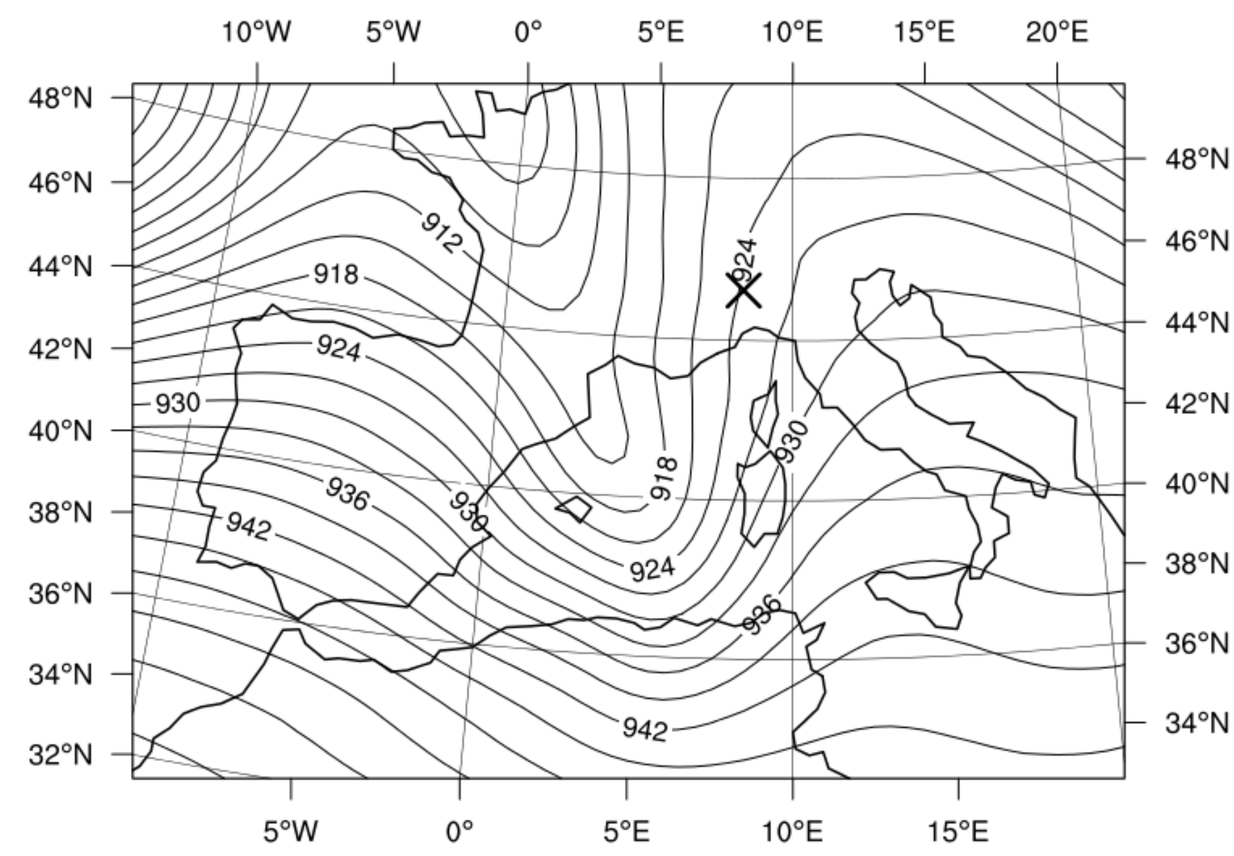
21-10-1999 h 06:00 UTC
10°W 5°W 0° 5°E 10°E 15°E 20°E
48°N 46°N 44°N 42°N 40°N 38°N 36°N 34°N 32°N
912 918 924 930 936 939 924 918 930 936 942 942

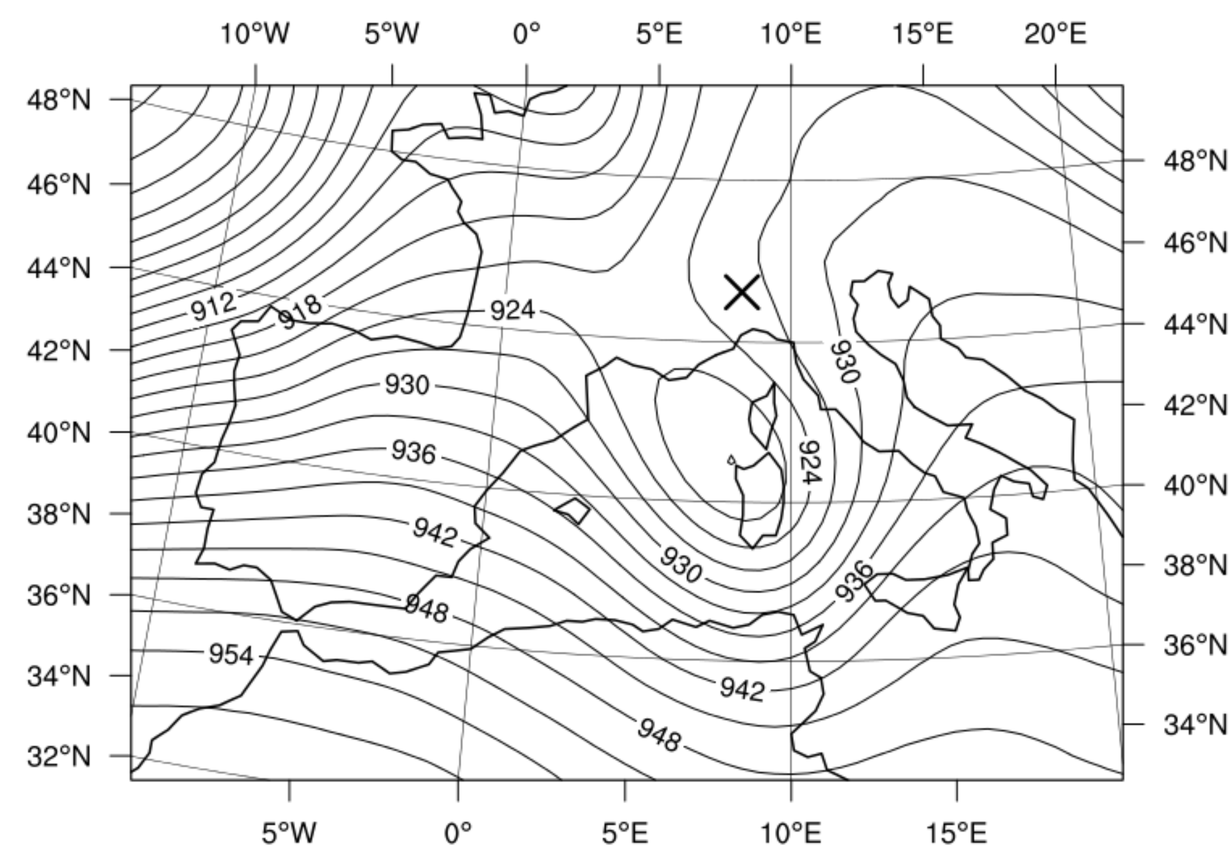
21-10-1999 h 12:00 UTC
10°W 5°W 0° 5°E 10°E 15°E 20°E
48°N 46°N 44°N 42°N 40°N 38°N 36°N 34°N 32°N
912 918 924 930 936 942 930 924 936 948 954 942 948

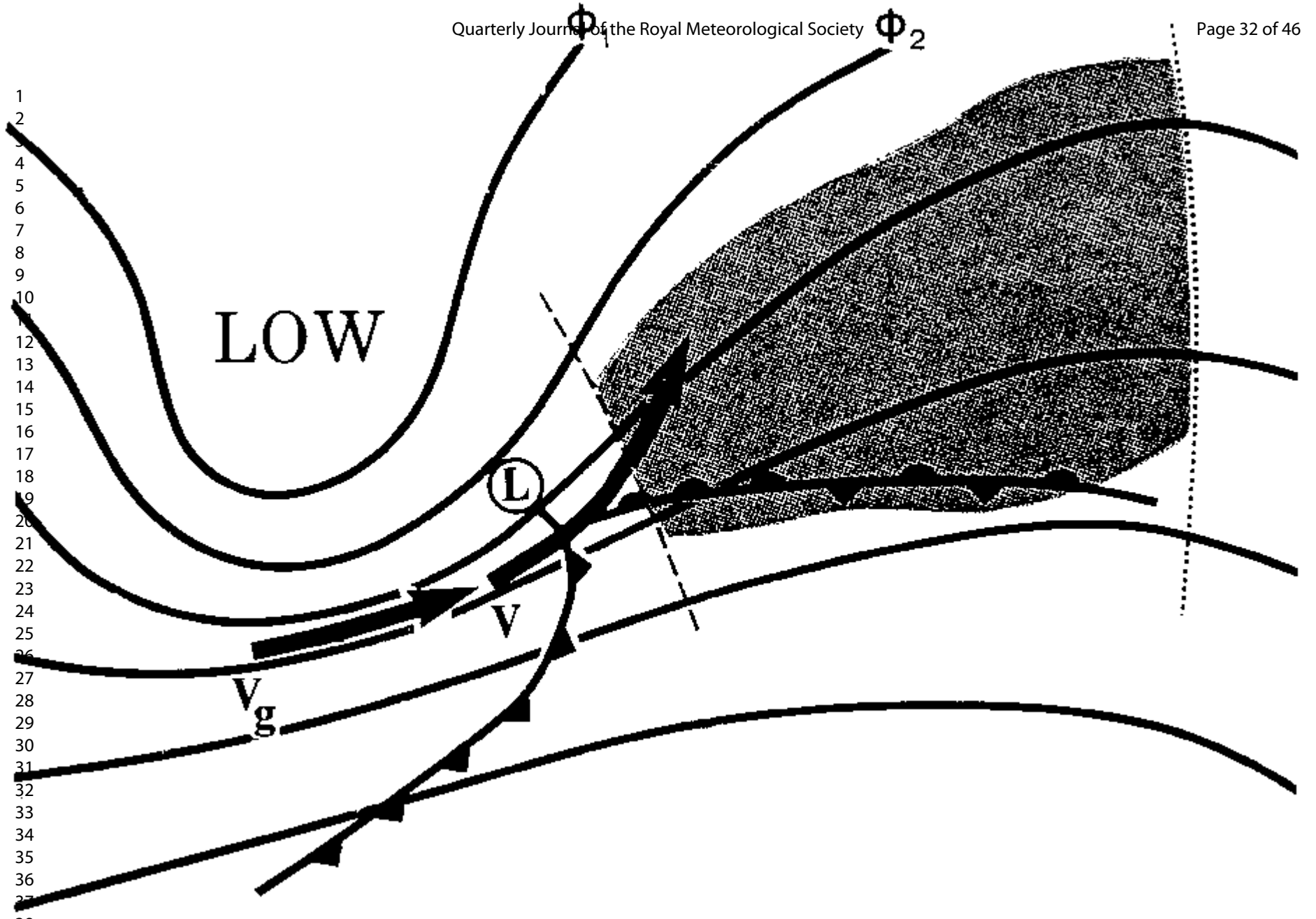
Φ1
Φ2
LOW
L
V
Vg

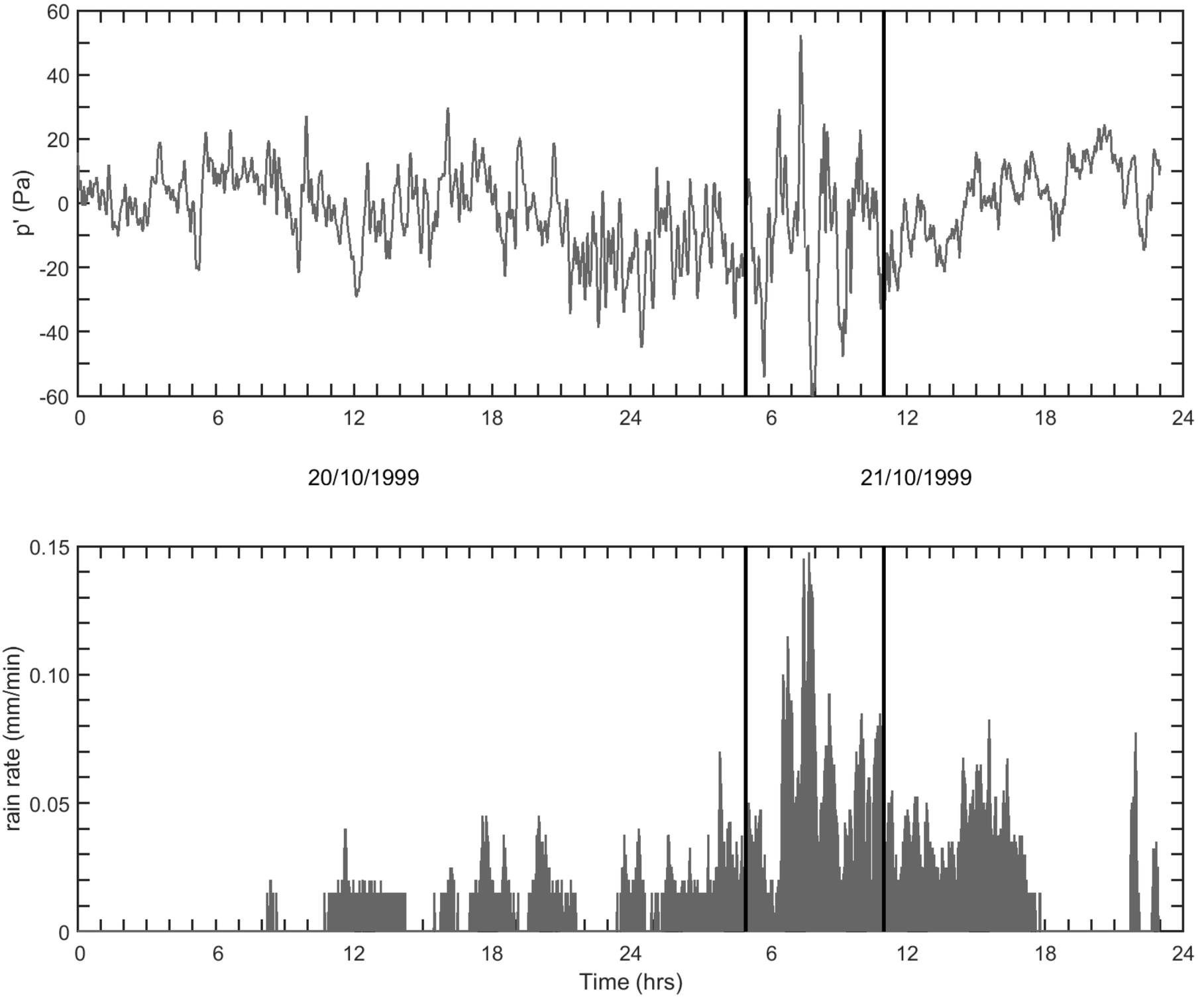
p' (Pa)
60
40
20
0
-20
-40
-60
0
6
12
18
24
6
12
18
24
20/10/1999
21/10/1999
rain rate (mm/min)
0.15
0.10
0.05
0
0
6
12
18
24
6
12
18
24
Time (hrs)

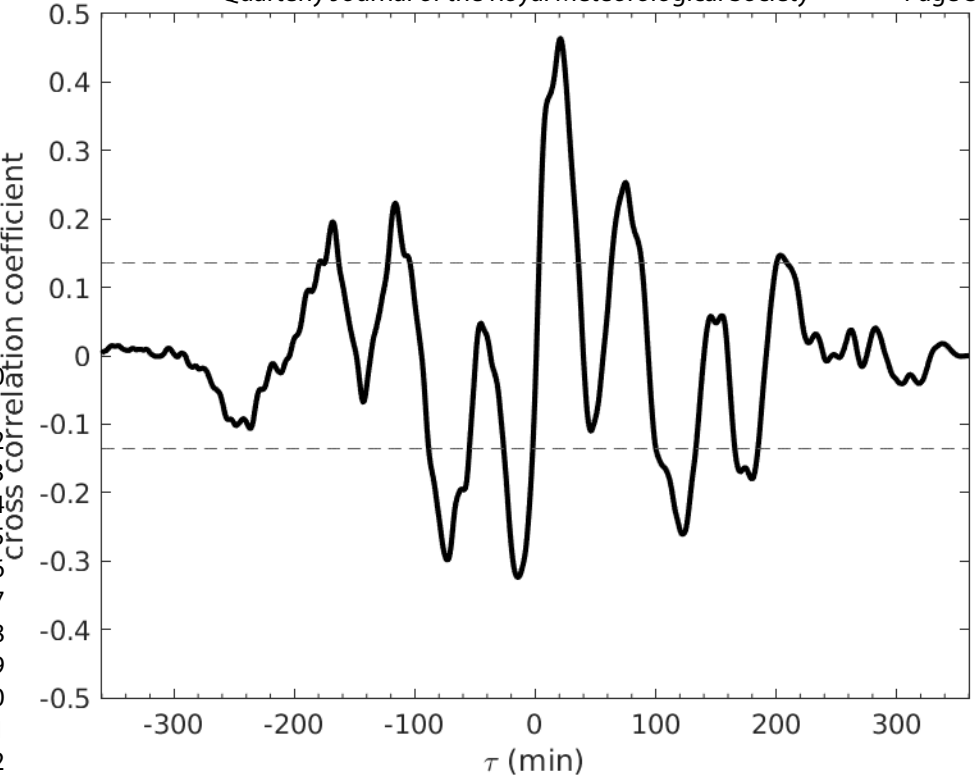
0.5
0.4
0.3
0.2
0.1
0
-0.1
-0.2
-0.3
-0.4
-0.5
cross correlation coefficient
-300
-200
-100
0
100
200
300
τ (min)

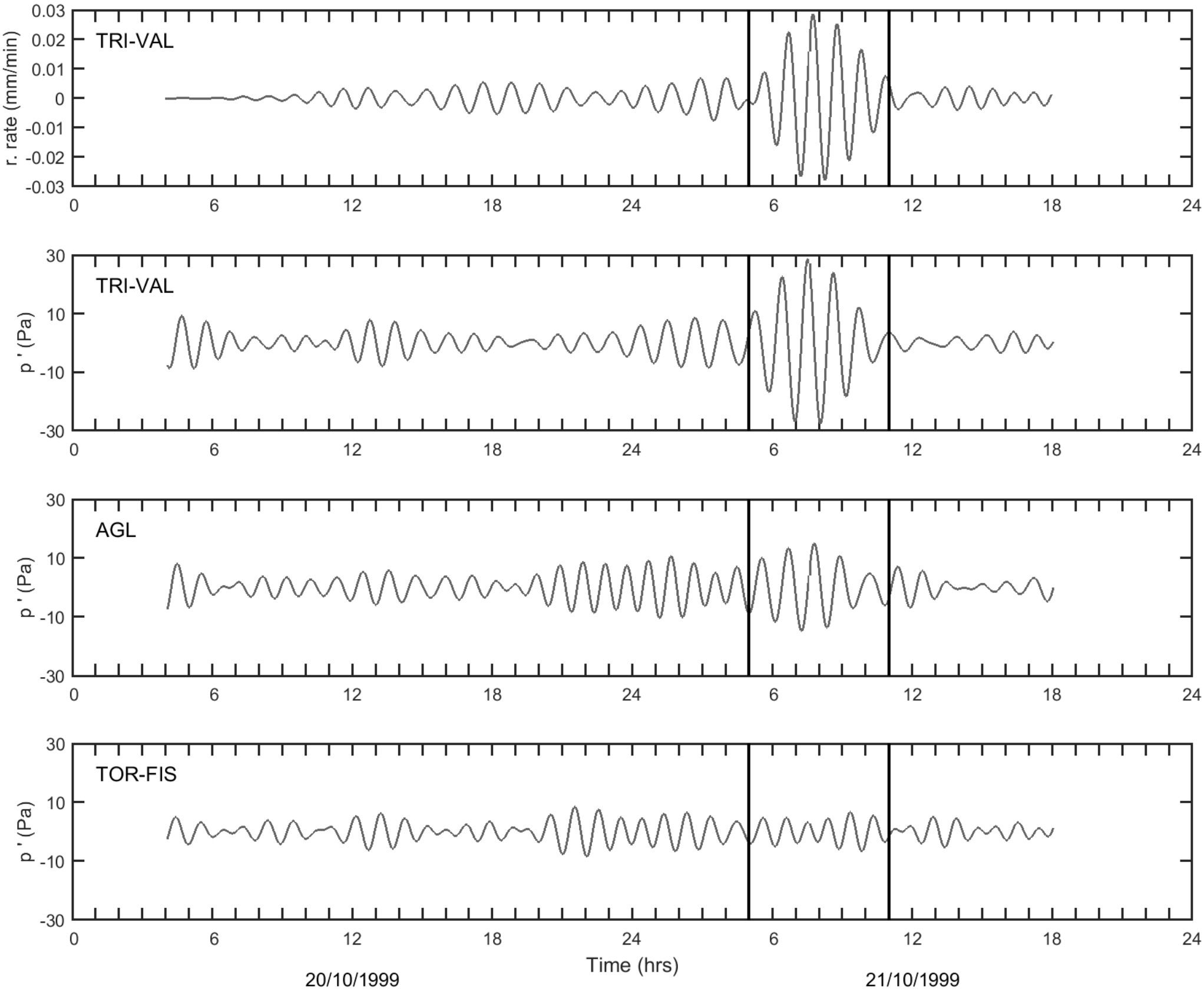
TRI-VAL
r. rate (mm/min)
0.03
0.02
0.01
0
-0.01
-0.02
-0.03
TRI-VAL
p ' (Pa)
30
10
-10
-30
AGL
TOR-FIS
0
6
12
18
24
Time (hrs)
20/10/1999
21/10/1999

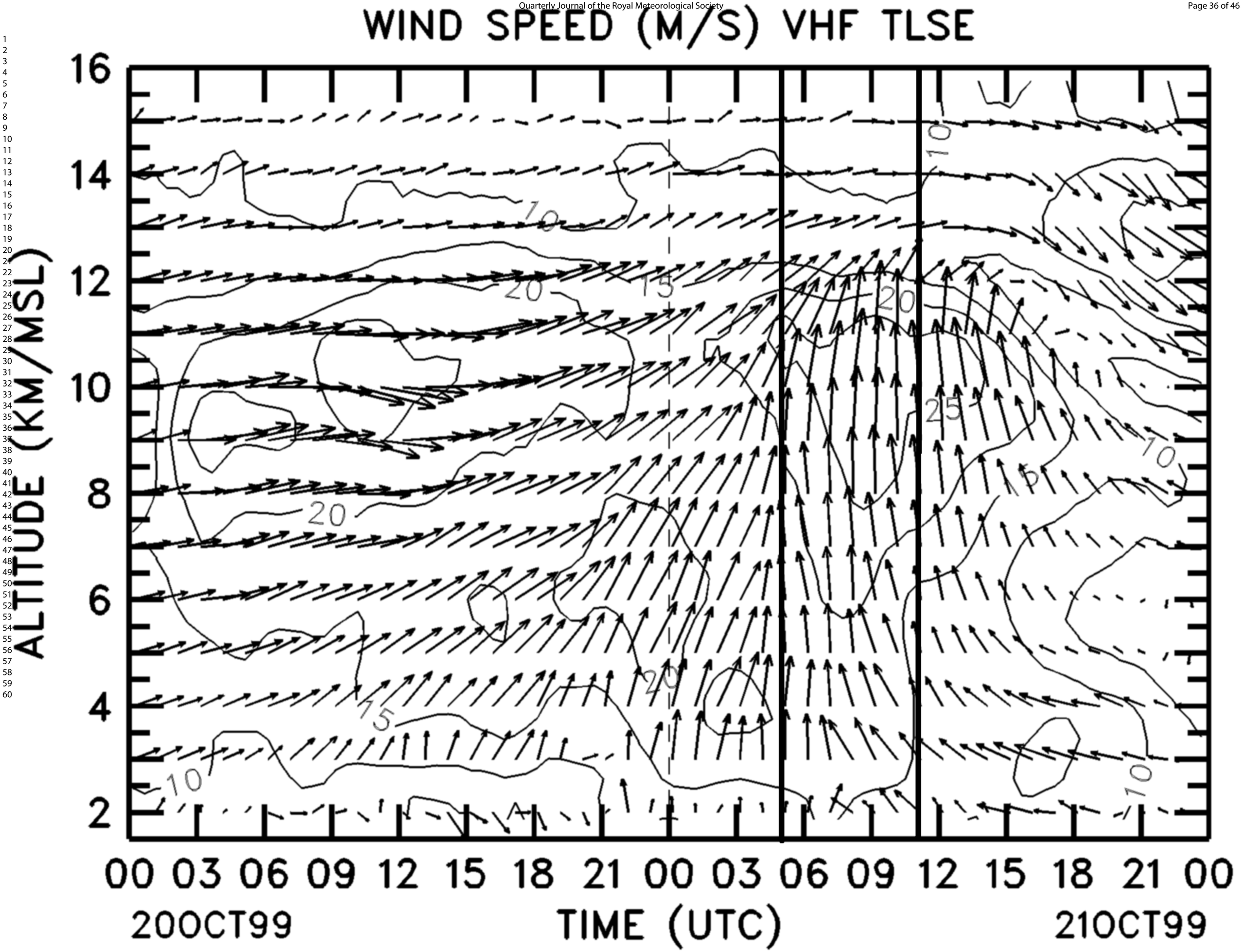
WIND SPEED (M/S) VHF TLSE
ALTITUDE (KM/MSL)
16
14
12
10
8
6
4
2
10
20
15
20
10
25
10
20
15
10
00 03 06 09 12 15 18 21 00 03 06 09 12 15 18 21 00
20OCT99
TIME (UTC)
21OCT99

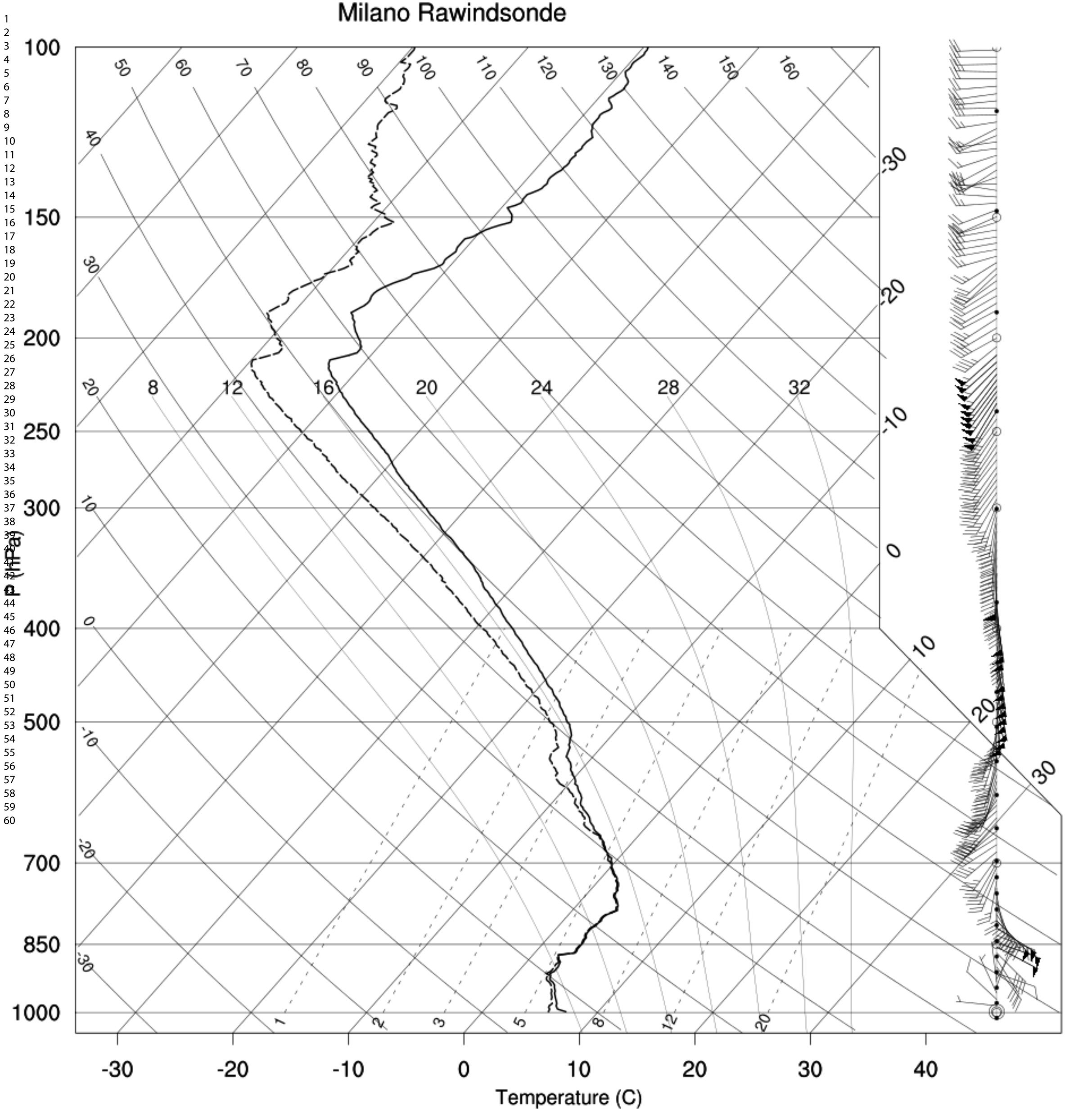
Milano Rawindsonde
p (hPa)
100
150
200
250
300
400
500
700
850
1000
-30
-20
-10
0
10
20
30
40
Temperature (C)

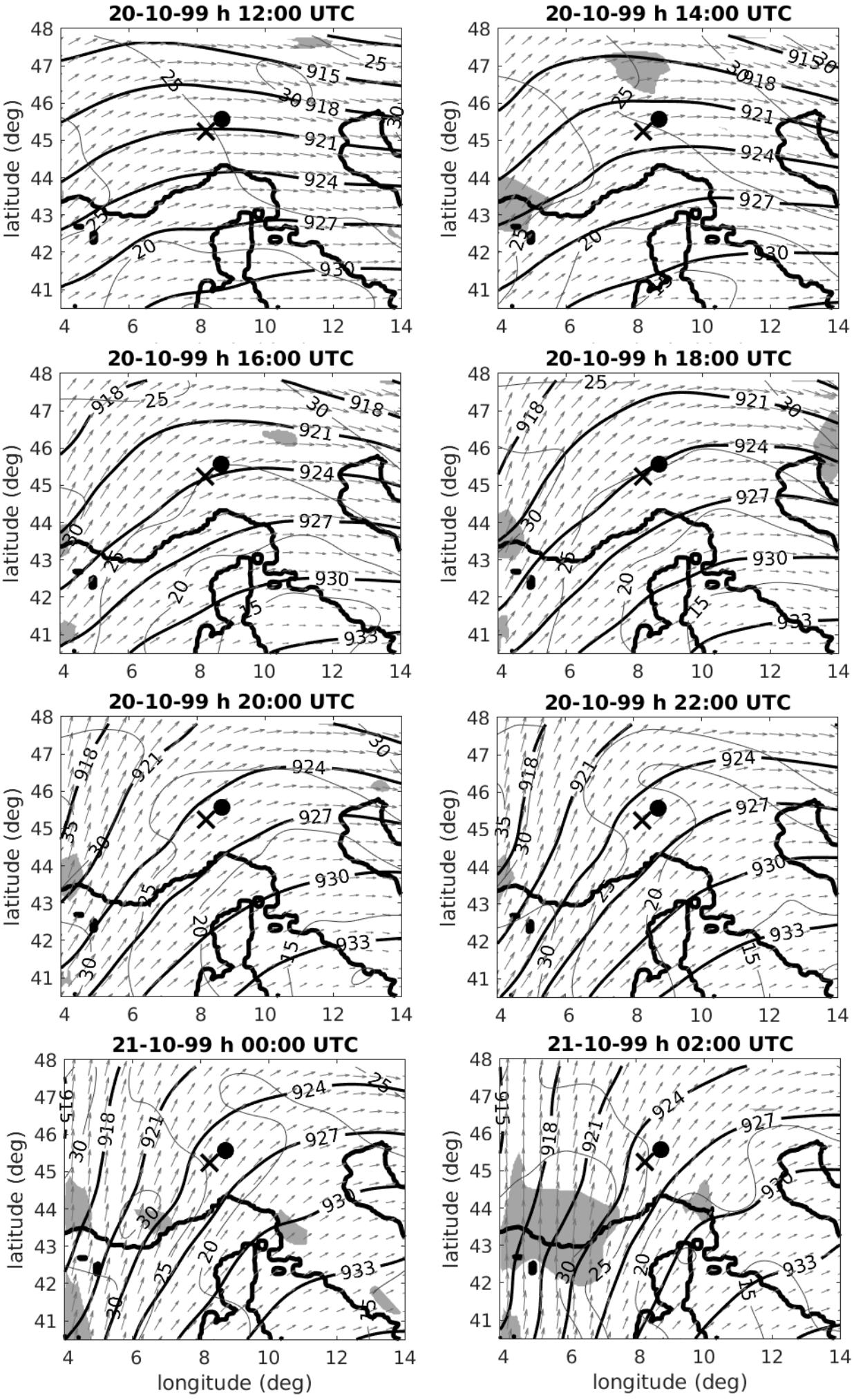
20-10-99 h 12:00 UTC
20-10-99 h 14:00 UTC
20-10-99 h 16:00 UTC
20-10-99 h 18:00 UTC
20-10-99 h 20:00 UTC
20-10-99 h 22:00 UTC
21-10-99 h 00:00 UTC
21-10-99 h 02:00 UTC
latitude (deg)
longitude (deg)

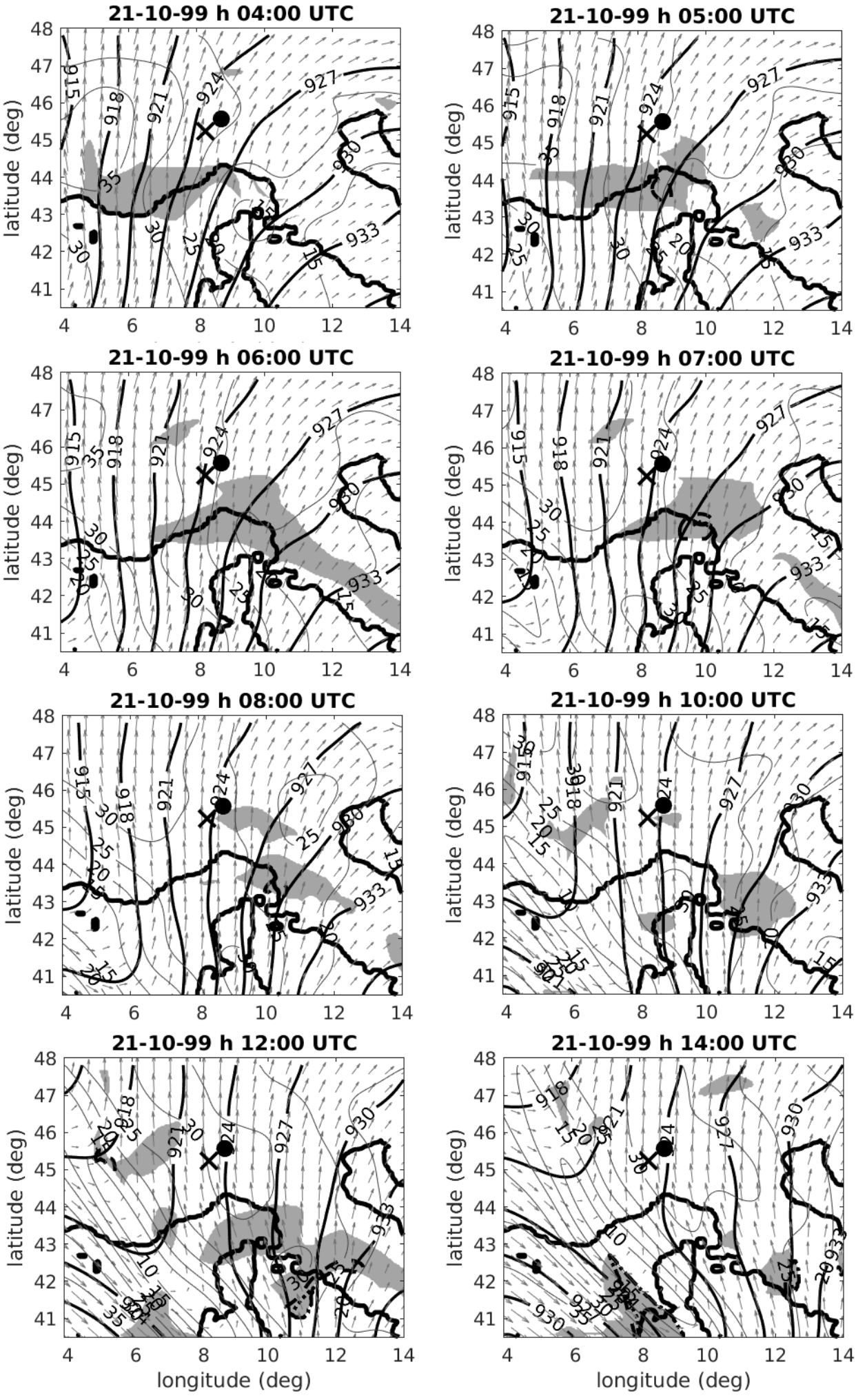
21-10-99 h 04:00 UTC
21-10-99 h 05:00 UTC
21-10-99 h 06:00 UTC
21-10-99 h 07:00 UTC
21-10-99 h 08:00 UTC
21-10-99 h 10:00 UTC
21-10-99 h 12:00 UTC
21-10-99 h 14:00 UTC
latitude (deg)
longitude (deg)

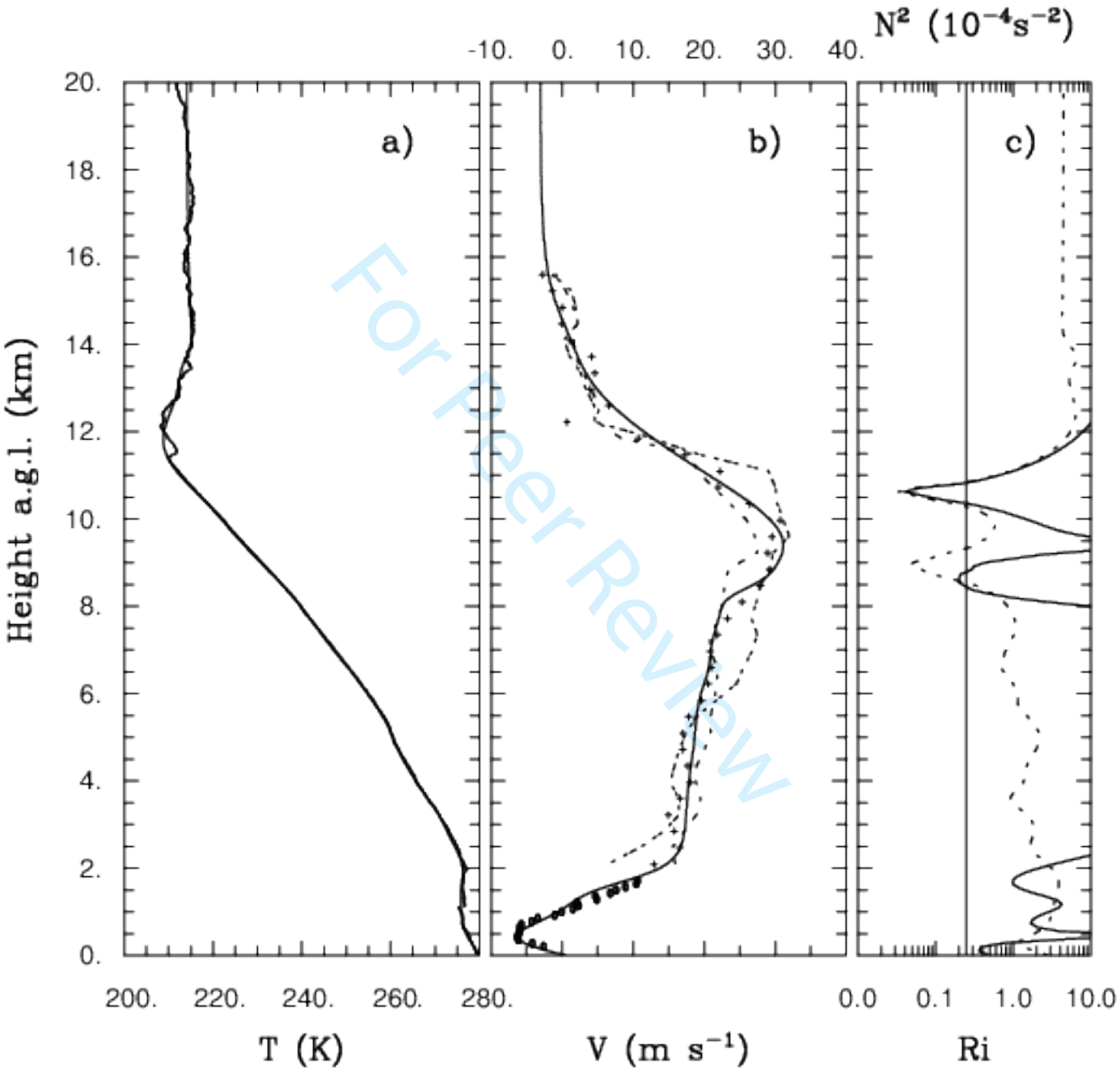

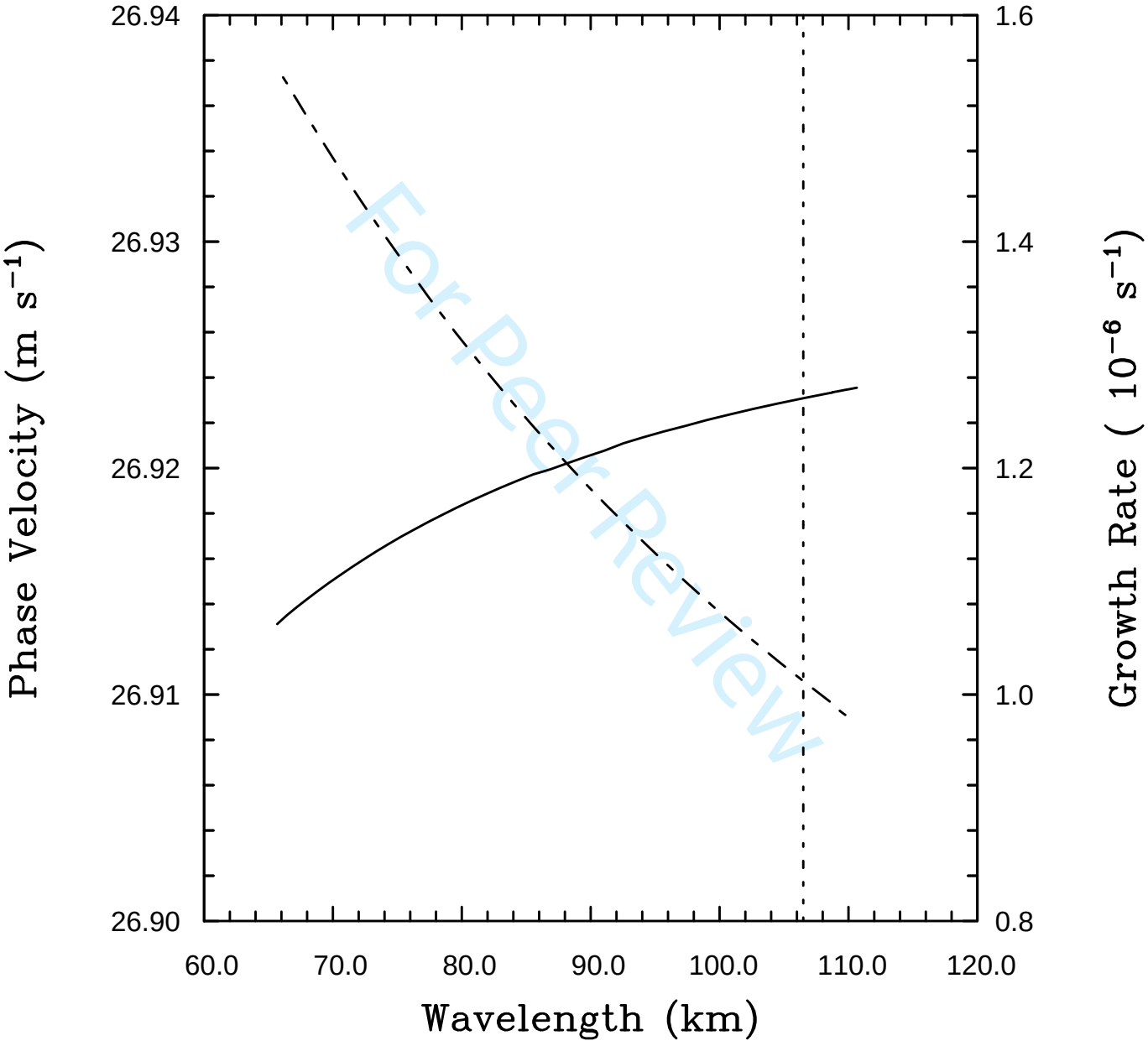

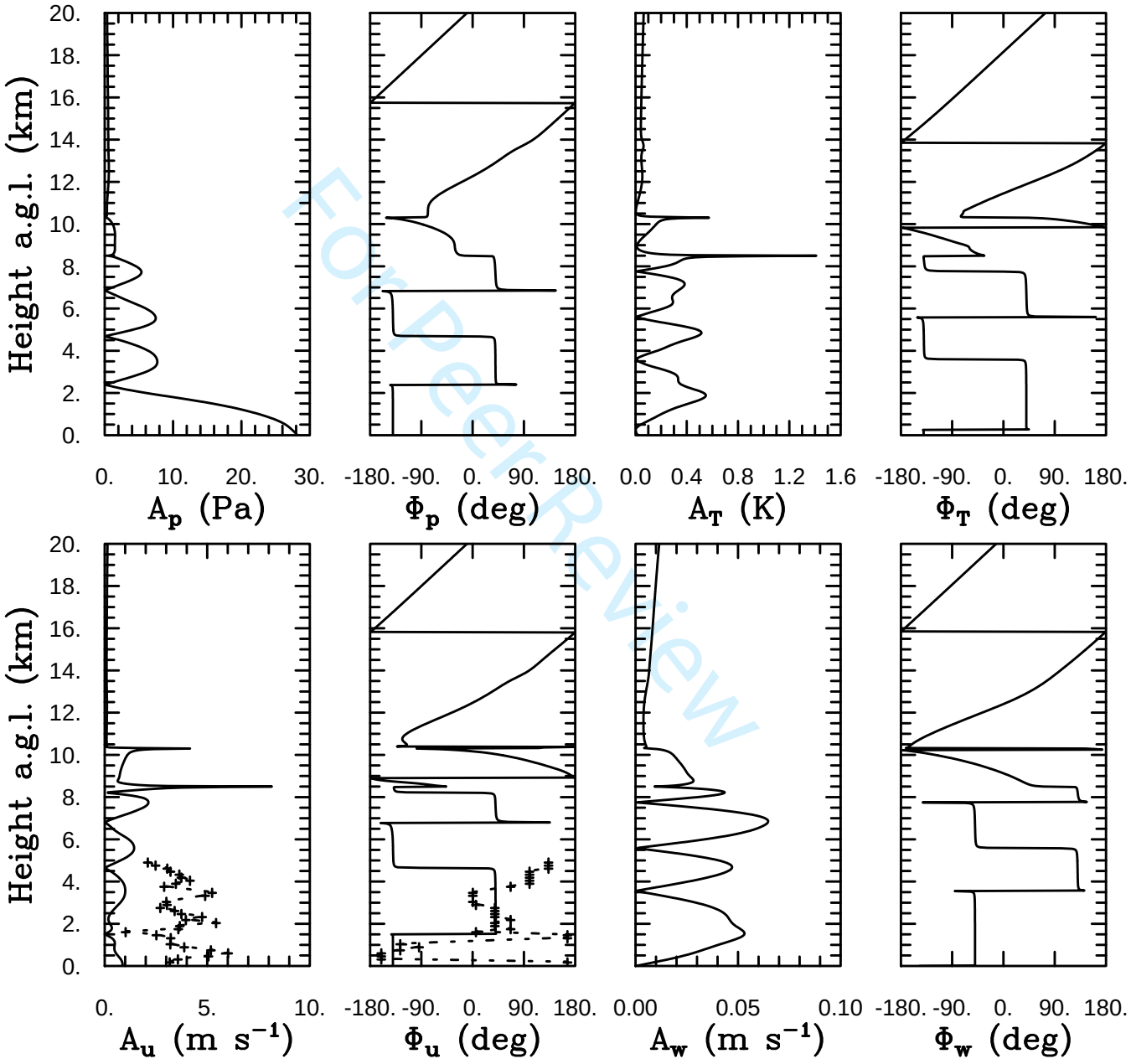

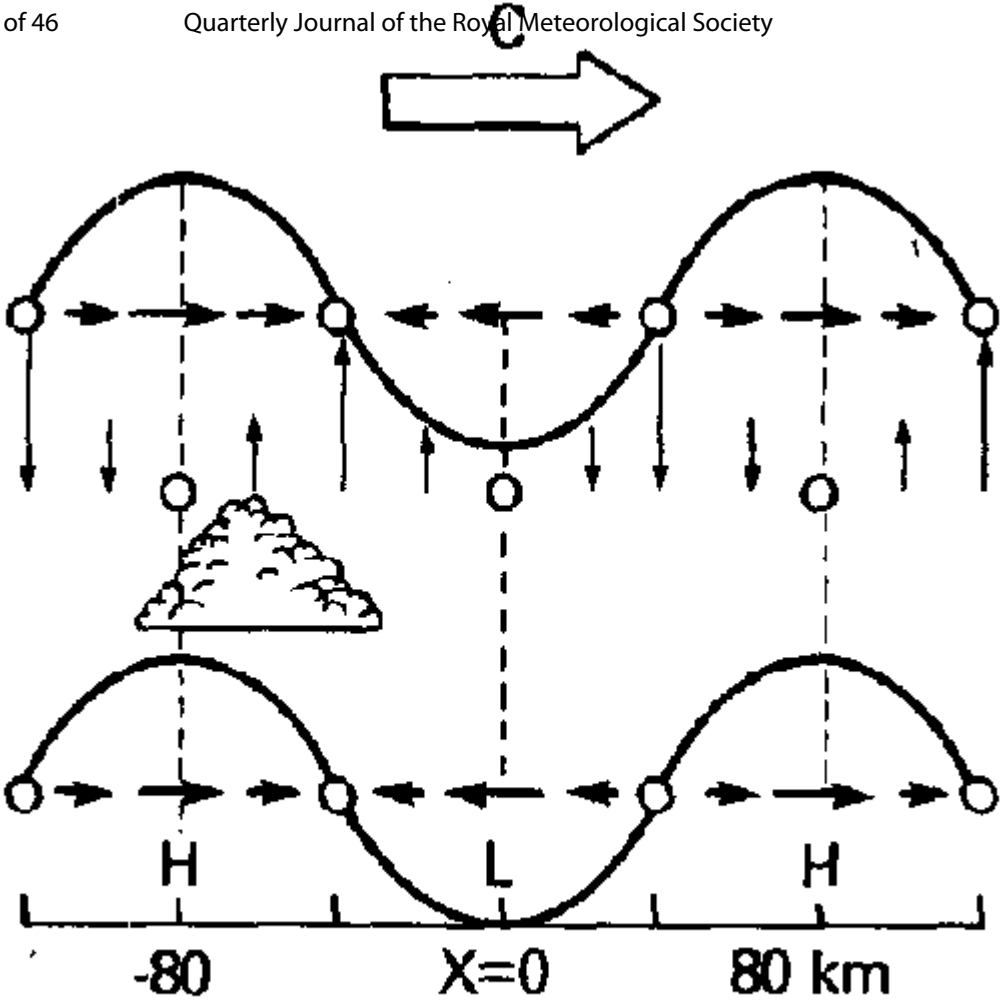

WAVE WITH NO TILT

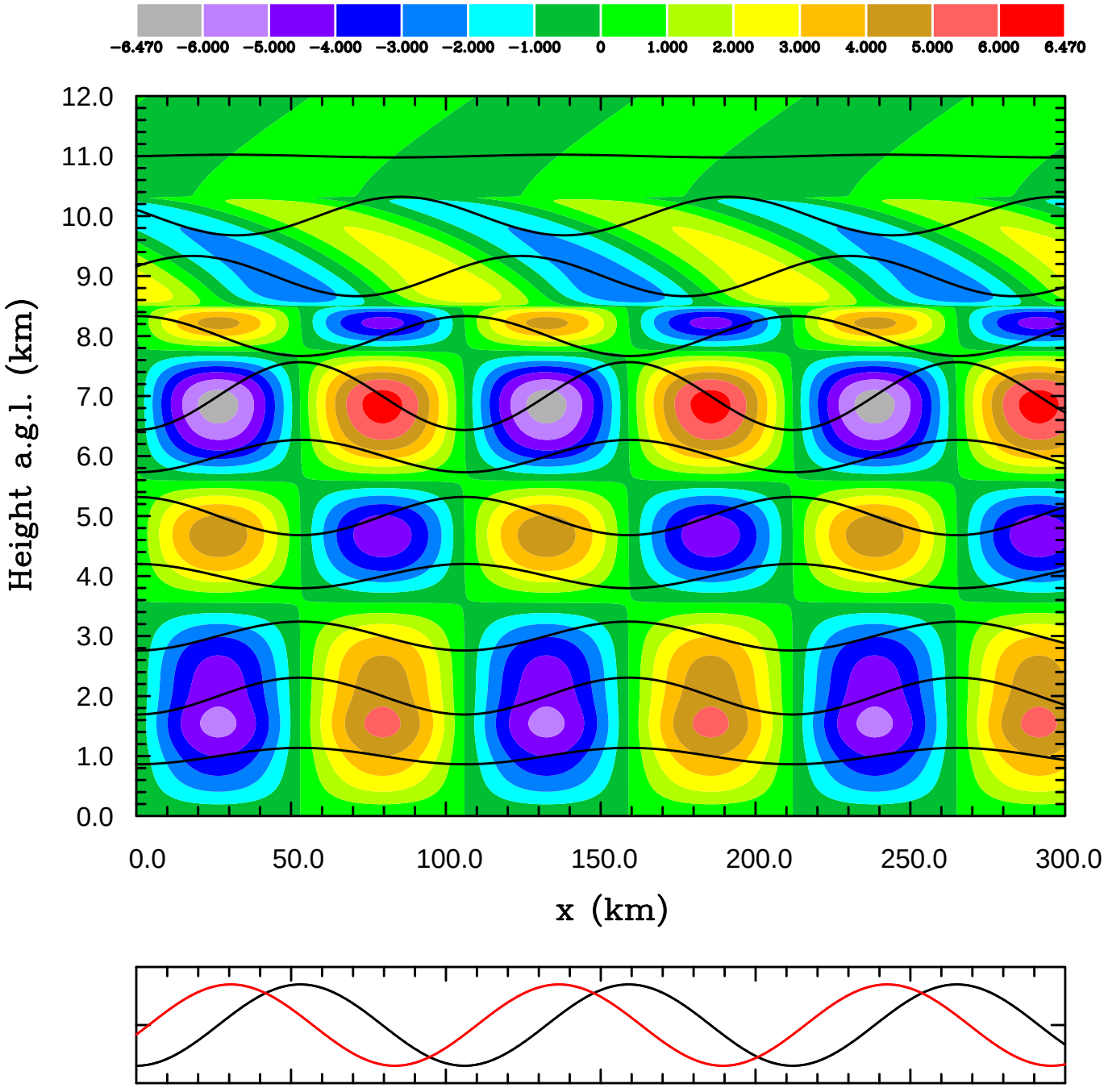
−6.470 −6.000 −5.000 −4.000 −3.000 −2.000 −1.000 0 1.000 2.000 3.000 4.000 5.000 6.000 6.470
Height a.g.l. (km)
12.0
11.0
10.0
9.0
8.0
7.0
6.0
5.0
4.0
3.0
2.0
1.0
0.0
0.0 50.0 100.0 150.0 200.0 250.0 300.0
x (km)

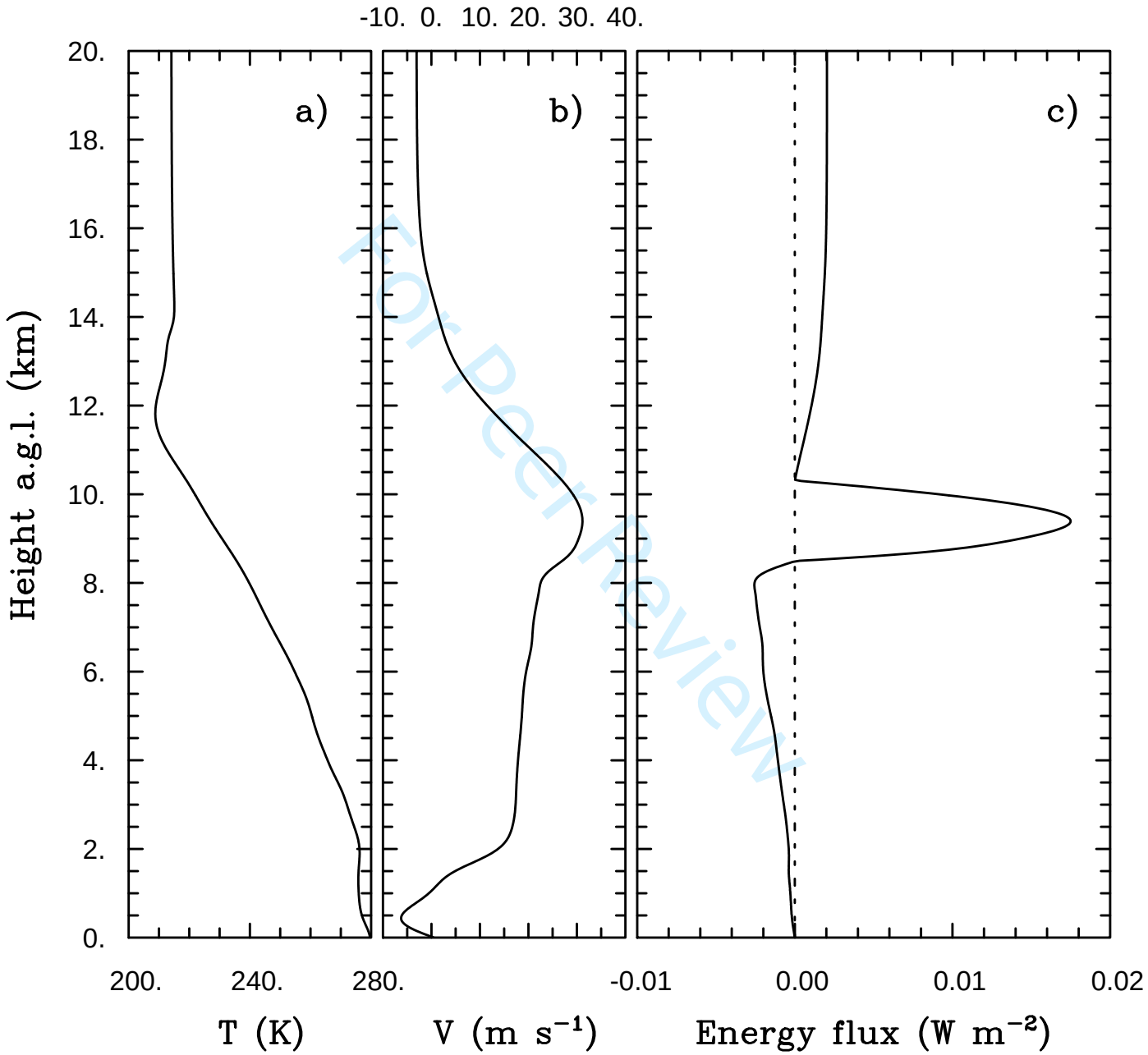

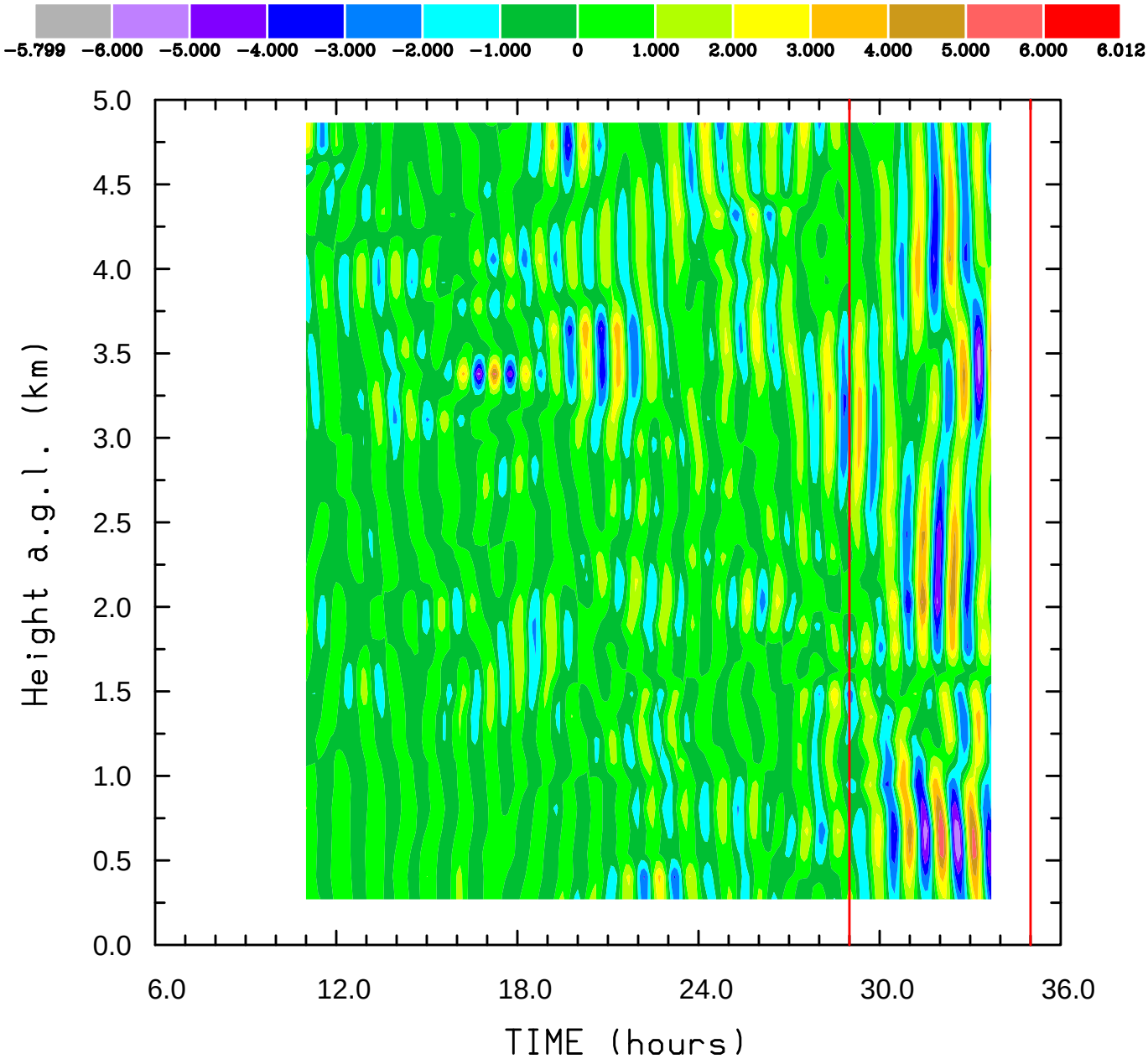
−5.799
−6.000
−5.000
−4.000
−3.000
−2.000
−1.000
0
1.000
2.000
3.000
4.000
5.000
6.000
6.012
Height a.g.l. (km)
5.0
4.5
4.0
3.5
3.0
2.5
2.0
1.5
1.0
0.5
0.0
6.0
12.0
18.0
24.0
30.0
36.0
TIME (hours)